Testing a one-closure equation turbulence model in neutral boundary layers

Roger Lewandowski, Benoît Pinier, Etienne Mémin, Pranav Chandramouli

Testing a one-closure equation turbulence model in neutral boundary layers

Roger Lewandowski*[1], Benoît Pinier[2], Etienne Mémin[3], and Pranav Chandramouli[4]

[1,2,3,4]IRMAR, UMR CNRS 6625, University of Rennes 1 and FLUMINANCE Team, INRIA Rennes, France

Abstract

We test the performances of an incompressible turbulence Reynolds-Averaged Navier-Stokes one-closure equation model in a boundary layer, which requires the determination of the mixing length ℓ. A series of direct numerical simulation are performed, with flat and non trivial topographies, to obtain by interpolation a generic formula $\ell = \ell(Re_\star, z)$, $Re_\star$ being the frictional Reynolds number, and z the distance to the wall. Numerical simulations are carried out at high Reynolds numbers with this turbulence model, in order to discuss its ability to properly reproduce the standard profiles observed in neutral boundary layers, and to assess its advantages, its disadvantages and its limits. In an appendix, we achieve the mathematical analysis of the model.

Key words : Fluid mechanics, Turbulence models, Navier-Stokes Equations, Direct numerical simulations, Boundary layer, Channel flows.

2010 MSC: 76D10, 76F40, 35Q30.

1 Introduction

The simulation of a turbulent flow by a direct numerical simulation (DNS) using the Navier-Stokes Equations (NSE) remains today out of reach for a high Reynolds number Re. Indeed, the Kolmogorov's laws imply that $O(Re^{9/4})$ degrees of freedom are necessary to do so, which is too large in term of computing power for realistic turbulent flows, such as geophysical flows, the Reynolds number of which is larger than 10^8. This is why turbulence models are always essential until now. Among all turbulence models, two main classes can be distinguished: the Large Eddy Simulation models (LES), such as Smagorinsky's model, and the Reynolds-Averaged Navier-Stokes (RANS) models, such as the $k-\varepsilon$ model [11, 25, 31, 33].

The aim of this paper is to investigate the ability of one of the most basic incompressible RANS model to faithfully reproduce a neutral boundary layer. The model under consideration is a by-product of the $k-\varepsilon$ model with only one closure equation, specified by the following PDE system:

$$(1.1)\quad \begin{cases} (\overline{\mathbf{v}}\cdot\nabla)\,\overline{\mathbf{v}} - \nabla\cdot\left[(2\nu + C_v\ell\sqrt{k})\,D\overline{\mathbf{v}}\right] + \nabla\overline{p} = \mathbf{f}, & (i)\\ \nabla\cdot\overline{\mathbf{v}} = 0, & (ii)\\ \overline{\mathbf{v}}\cdot\nabla k - \nabla\cdot((\mu + C_k\ell\sqrt{k})\nabla k) = C_k\ell\sqrt{k}|D\overline{\mathbf{v}}|^2 - \ell^{-1}k\sqrt{|k|}, & (iii)\end{cases}$$

*Corresponding author: Roger.Lewandowski@univ-rennes1.fr

where "$\nabla\cdot$" is the divergence operator and

i) $\overline{\mathbf{v}} = (\overline{u}, \overline{v}, \overline{w})$ is the long time average of the flow [4, 20] (or any stationary statistical mean, which does not make any difference thanks to the ergodic assumption about turbulent flows, see for instance in [14]), $\overline{p}$ the mean pressure, k the turbulent kinetic energy (TKE), $D\overline{\mathbf{v}} = (1/2)(\nabla\overline{\mathbf{v}} + \nabla\overline{\mathbf{v}}^T)$ the deformation tensor,

ii) $\nu > 0$ is the kinematic viscosity of the flow, $\mu > 0$ a diffusion coefficient, $\mathbf{f}$ a source term expressing possible external forces,

iii) $\nu_t = C_v \ell\sqrt{k}$ is the eddy viscosity, $\mu_t = C_k \ell\sqrt{k}$ the eddy diffusion, ℓ the Prandtl mixing length, $C_v > 0$ and $C_k > 0$ are dimensionless constants,

iv) the term $C_k \ell\sqrt{k}|D\overline{\mathbf{v}}|^2$ in the equation (1.1, (iii)) is the dissipation of the mean flow, generating turbulent kinetic energy, whereas $\varepsilon = \ell^{-1} k\sqrt{|k|}$ is the mean dissipation of the fluctuations, damping the TKE.

This type of one-closure equation model can be a good alternative to the full two-closure equations $k-\varepsilon$ model, which is expensive and very hard to implement numerically, although very accurate and effective. Evolutionary versions of (1.1) have been used for large scale oceanic simulations ([5, 22]), and also in marine engineering to simulate a 2D flow around a fishing net [24].
A natural question is: how far can such one-closure model be used instead of the full $k-\varepsilon$ model or higher order closure models such as the Melor-Yamada model [12] ? It depends strongly on how the mixing length ℓ and the boundary conditions are set.
In [24], 2D simulations are performed at $Re = 10^5$ around, with ℓ chosen equal to the local size of the mesh. The no slip boundary condition for $\overline{\mathbf{v}}$ was applied combined with homogenous Dirichlet boundary condition for k. Although we got very good results, it will not work for a 3D boundary layer. Therefore, alternative options have to be tested.
To fix ideas, let us consider a 3D flow over a plate, placed at $z = 0$. The flow domain is the half space $\{z \geq 0\}$, divided in two regions:

i) the boundary layer $\{0 \leq z \leq z_0\}$, z_0 being the height of the boundary layer,

ii) $\{z_0 \leq z\}$, where a turbulent model is implemented.

At $z = z_0$, the boundary condition satisfied by the mean velocity is usually a wall law, one of the most popular being the Glaucker-Manning law (see in [11, Chapter 5])[1]:

$$\overline{\mathbf{v}} \cdot \mathbf{n} = 0, \quad -[(2\nu + \nu_t) D\overline{\mathbf{v}} \cdot \mathbf{n}]_\tau = \alpha_v |\overline{\mathbf{v}}| \overline{\mathbf{v}}. \tag{1.2}$$

When the model involves the TKE, people used to set, at $z = z_0$,

$$k = |\overline{\mathbf{v}}|^2. \tag{1.3}$$

The boundary layer is often modeled by a given continuous steady profile depending on z, most of the time linear in the viscous sublayer and then logarithmic. However, there are several different models [11, 34, 35], more or less sophisticated, depending on the desired degree of accuracy and the available computing power. When stratification occurs, such as in the atmosphere, the Monin Obukhov theory [26] applies, requiring addition of stabilizing functions to the log profile, which may be controversial [29]. Moreover, in

[1] Let $\mathbf{n}$ denotes the outward normal vector at the boundary, and for a given vector $\mathbf{w}$, $\mathbf{w}_\tau = \mathbf{w} - (\mathbf{w}\cdot\mathbf{n})\mathbf{n}$ its tangential part. We refer to ν_t as any eddy viscosity.

the case of the ocean, there are many other boundary layer models, as for instance the Pacanowski-Philander model, based on closure equations with eddy viscosities, functions of the Richardson number [3].
Therefore, there is no universal boundary layer model. This is what motivates us to evaluate the performances of the model (1.1) inside a boundary layer, which means taking z_0 at least of order of the height of the viscous sublayer. We will do so in the case of a flat bottom, then in the case of a non trivial topography as displayed in figure 1, called the rough case.

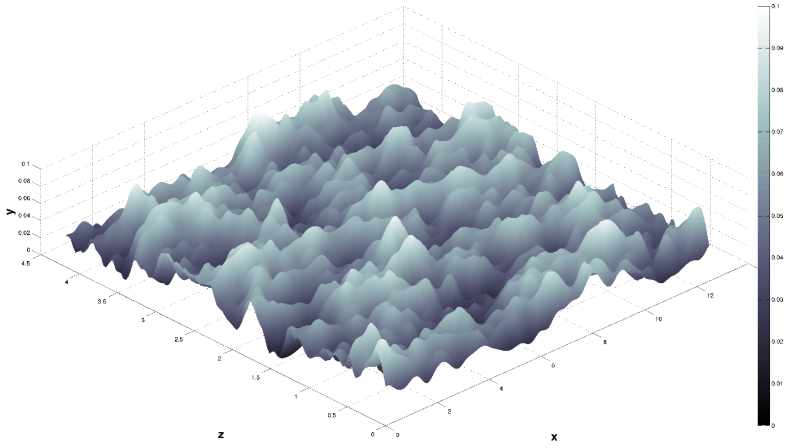

Figure 1: Non trivial topography, also called the rough case.

A natural option is solving (1.1) with the boundary conditions (1.2)-(1.3) inside the boundary layer, provided that the mixing length ℓ is specified. However, we know that the resulting boundary value problem, for a given smooth function $\ell = \ell(\mathbf{x})$, yields serious mathematical and numerical complications (see in [11, Chapters 7,8] and additional comments in section A.1 below), mainly because of (1.3), that must be reconsidered. In this perspective, we have modeled in this paper an alternative boundary condition for the TKE k, which is a non linear Neumann boundary condition, see (2.13) below. We get a more affordable mathematical structure than that provided by (1.3) (see Appendice A). The resulting model, (1.1)-(1.2)-(2.13), is appointed by the acronym NSTKE.
For running the NSTKE model, the mixing length ℓ must be determined. In the full $k-\varepsilon$ model, it is deduced from k and ε by the standard formula

$$\ell = \frac{k^{3/2}}{\varepsilon}, \tag{1.4}$$

which cannot be directly used in our NSTKE model, since we do not have any equation to compute ε. We get numerical values of ε from direct numerical simulations (DNS) using the Navier-Stokes equations at some low and medium Reynolds numbers. To be more specific, let $Re_\star$ denotes the frictional Reynolds number (see definition (3.1) below). By the formula (1.4) and assuming that ℓ is homogeneous in the $x-y$ axes, we evaluate $\ell = \ell(z, Re_\star)$ at the grid points, properly averaging the data based on the DNS. We then interpolate the collected sets of numerical values to get a general formula in both flat and rough cases (see formula (3.17) and (3.18), complemented by (3.19), (3.21) and (3.22) for

the calculation of the different coefficients)[2]. Our DNS are compared to the DNS of Moser et al. [18, 27], which serve as the benchmark for our results.
With this formula for ℓ, several numerical simulations with the NSTKE model have been performed up to $Re_\star = 10000$, in both flat and rough cases, after having evaluated the roughness coefficients contained in the boundary conditions. There is no universal turbulence model, and this one is neither better nor worse than another. The approach to use it for numerical simulations is as important as the model itself.
The NSTKE model behaves properly in the flat case, which validates our approach. However, the results are less good in the rough case. This does not mean that the model and our approach have reached their limits, and the present study opens several questions. We clearly do not have enough DNS in the rough case for the determination of ℓ. Moreover, in this case, the assumption $\ell = \ell(z, Re_\star)$ must be called into question, in favour of $\ell = \ell(x, y, z, Re_\star)$. Last but not least, this first series of results shows that the topography should be strongly taken into account in the calculation of the roughness coefficients, and it remains an open question to know how to find a universal and simple way for doing this, which is one of the main challenge in the field (see the "bulk algorithm" in [29] for instance).
This paper is a snapshot of a constantly evolving research. It is organized as the introduction, in the following order: TKE boundary condition modeling, DNS and mixing length formula, NSTKE simulations and analysis of the results and convergence. The paper is ended by an appendix, in which one proves the existence of a weak solution to the NSTKE model, by a proof that can be extended to the evolutionary case, which is a clear theoretical advantage of the model.

2 Boundary condition modeling

The aim of this section is the derivation of the boundary condition (2.12) for the turbulent kinetic energy, TKE in the following. Before doing this, we set up the geometrical framework and recall the classical log law of the boundary layer mean velocity profil.

2.1 Geometry and boundary layers assumptions

The computational box Ω is defined by (see figure 2)

$$\Omega = [0, L_x] \times [0, L_y] \times [0, L_z].$$

For simplicity, we assume that the flow field $(\overline{\mathbf{v}}, \overline{p}, k)$ satisfies periodic boundary conditions in the x and y directions. To be more specific, $(\overline{\mathbf{v}}, \overline{p}, k)$ is defined on $\mathbb{R}^2 \times [0, L_z]$, and when it is at least of class C^2, for $\psi = \overline{\mathbf{v}}, \overline{p}, k$,

$$\forall\, (m, n) \in \mathbb{N}^2, \quad \forall\, (x, y, z) \in \Omega, \quad \psi(x + nL_x, y + mL_y, z) = \psi(x, y, z). \tag{2.1}$$

To carry out the modeling process, we assume that in the boundary layer, the mean velocity $\overline{\mathbf{v}}$ has a constant direction, $\overline{\mathbf{v}} = (\overline{u}, 0, 0)$, and is homogeneous in the x-y axes. Therefore, $\overline{u} = \overline{u}(z)$, which is a standard assumption.

[2] In the process, we also calculate the values of the constants C_v and C_k involved in the eddy viscosities

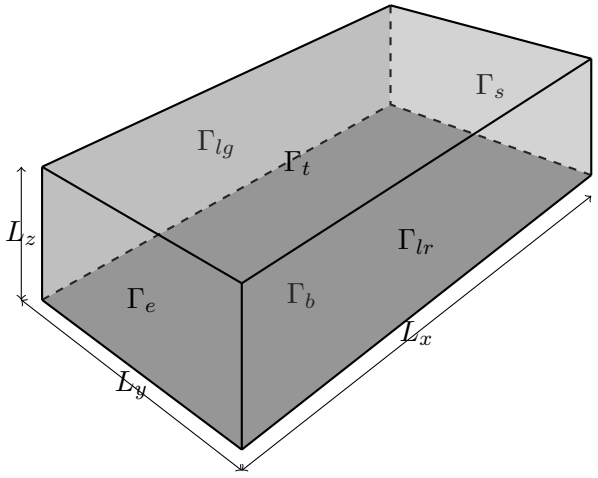

Figure 2: 3D Representation of Ω

It is generally accepted [11, 22, 25, 31] that there exists $0 < z_0 << z_1$ such that in the absence of stratification or buoyancy effects, $\overline{u}$ has in $[0, z_1]$ the following profile,

$$\forall\, z \in [0, z_0], \qquad \overline{u}(z) = \frac{u_\star}{\kappa}\frac{z}{z_0}, \tag{2.2}$$

$$\forall\, z \in [z_0, z_1], \qquad \overline{u}(z) = \frac{u_\star}{\kappa}\left(\log\left(\frac{z}{z_0}\right) + 1\right), \tag{2.3}$$

where $u_\star$ denotes the friction velocity, given by

$$u_\star = \sqrt{\nu \frac{\partial \overline{u}}{\partial z}(0)}, \tag{2.4}$$

and κ is the Van Karmàn constant, the numerical value of which is estimated between 0.35 and 0.42 [36]. Here z_1 denotes the height of the boundary layer.

2.2 Boundary condition for the TKE

We model in this section a boundary condition for the TKE at $z = z_0$, alternative to (1.3). In order to proceed, we first must:

i) Determine the eddy diffusion coefficient μ_t in $[0, z_0]$,

ii) Settle the profile of the TKE k in the same region, in which we assume $k = k(z)$.

i) According to standard use, we assume that in $[0, z_0]$, the flow is driven by the mixing length ℓ and the friction velocity $u_\star$, and that

$$\ell = \kappa z.$$

Therefore, as z and $u_\star$ are dimensionally independent, $(z, u_\star)$ is a dimensional basis (see [11, Chapter 3]). We deduce from straightforward calculation based on dimensional analysis the usual formula:

$$\forall\, z \in [0, z_0], \quad \mu_t(z) = \kappa_\mu u_\star z, \tag{2.5}$$

where κ_μ is a dimensionless constant.
ii) It is natural to set $k(0) = 0$ and $k(z_0) = \overline{u}^2(z_0)$, which yields, by (2.2),

$$k(0) = 0, \quad k(z_0) = \frac{u_\star^2}{\kappa^2}. \tag{2.6}$$

Following (2.2) we enforce k to be linear in the viscous sublayer[3], which leads by (2.6) to

$$\forall\, z \in [0, z_0], \quad k(z) = \frac{u_\star^2}{\kappa^2}\frac{z}{z_0}. \tag{2.7}$$

We derive from these modeling hypotheses, the following result.

Proposition 2.1. *Assume that (2.7) and (2.5) hold. Then the following expansion holds:*

$$\forall\, z \in]0, z_0], \quad \mu_t \frac{dk}{dz} = \kappa\kappa_\mu \left(\frac{z_0}{z}\right)^{\frac{1}{2}} k\sqrt{k} + o(z). \tag{2.8}$$

Proof. We expand $k(z)$ between 0 and z:

$$k(0) = k(z) - z\frac{dk}{dz}(z) + o(z). \tag{2.9}$$

By (2.7), we get

$$z\frac{dk}{dz}(z) = \frac{u_\star^2}{\kappa^2}\left(\frac{z}{z_0}\right) + o(z). \tag{2.10}$$

We combine (2.5) and (2.10), and we get

$$\mu_t \frac{dk}{dz}(z) = \frac{\kappa_\mu}{\kappa^2} u_\star^3 \left(\frac{z}{z_0}\right) + o(z). \tag{2.11}$$

The relation (2.7) can be rewritten for $z > 0$ as

$$u_\star = \kappa \left(\frac{z_0}{z}\right)^{\frac{1}{2}} \sqrt{k(z)},$$

that we insert in (2.11) to eliminate $u_\star$, which yields (2.8). □

When we neglect the remaining term in (2.8), we get at $\Gamma_{b,c} = \{z = z_0\}$ the following boundary condition for k:

$$\mu_t \frac{dk}{dz} = \alpha_k k\sqrt{k}, \tag{2.12}$$

where $\alpha_k = \kappa\kappa_\mu$. By symmetry, a similar analysis can be carried out at the top of the computational box. Therefore, we can summarize the results in the following general setting:

$$-\mu_t \frac{\partial k}{\partial \mathbf{n}} = \alpha_k k\sqrt{k} \quad \text{at} \quad \mathbb{R}^2 \times (\{z = z_0\} \cup \{z = L_z - z_0\}) = G_c. \tag{2.13}$$

[3]Notice that, even it seems reasonable, this is an arbitrary choice, and that another choice would yields another boundary condition.

Remark 2.1. *Note that according to formula (1.4), the boundary condition (2.13) can be rewritten as*

$$-\mu_t \frac{\partial k}{\partial \mathbf{n}} = \alpha_k \ell \varepsilon. \tag{2.14}$$

This is as if at the computational boundary G_c, we decided that the TKE is damped by the mean dissipation of the fluctuation scaled by the mixing length, which is in coherence with the TKE equation and some way of a physical interpretation.

Let Om_c denotes the infinite strip

$$\mathrm{Om}_c = \mathbb{R}^2 \times [z_0, L_z - z_0]. \tag{2.15}$$

We are led to introduce the following boundary value problem:

$$\left\{ \begin{array}{rcll} (\overline{\mathbf{v}} \cdot \nabla)\, \overline{\mathbf{v}} - \nabla \cdot [(2\nu + \nu_t(k))\, D\overline{\mathbf{v}}] + \nabla p &=& \mathbf{f} & \text{in } \mathrm{Om}_c, \\ \nabla \cdot \overline{\mathbf{v}} &=& 0 & \text{in } \mathrm{Om}_c, \\ \overline{\mathbf{v}} \cdot \nabla k - \nabla \cdot [(\mu + \mu_t(k) \nabla k] &=& \nu_t(k) |D\overline{\mathbf{v}}|^2 - \ell^{-1} k \sqrt{|k|} & \text{in } \mathrm{Om}_c, \\ -[(2\nu + \nu_t(k)) D\overline{\mathbf{v}} \cdot \mathbf{n}]_\tau &=& \alpha_v |\overline{\mathbf{v}}| \overline{\mathbf{v}} & \text{on } G_c, \\ \overline{\mathbf{v}} \cdot \mathbf{n} &=& 0 & \text{on } G_c, \\ -(\mu + \mu_t(k)) \nabla k \cdot \mathbf{n} &=& \alpha_k k \sqrt{|k|} & \text{on } G_c, \end{array} \right. \tag{2.16}$$

with periodic boundary conditions in the x and y axes, as defined by (2.1). The proof of the existence of a weak solution to the system (2.16) is postponed to appendice A.

Remark 2.2. *We have replaced μ_t by $\mu + \mu_t$ to avoid degeneration issues in the TKE part of the system, where $\mu > 0$ is a small stabilizing mathematical parameter.*

Remark 2.3. *In the context of the modeling assumptions of this section, the wall law (1.2) becomes*

$$(2\nu + \nu_t) \frac{\partial \overline{u}}{\partial z} = \alpha_v \overline{u}^2 \quad at \quad z = z_0, \tag{2.17}$$

$$(2\nu + \nu_t) \frac{\partial \overline{u}}{\partial z} = -\alpha_v \overline{u}^2 \quad at \quad z = L_z - z_0. \tag{2.18}$$

Remark 2.4. *The coefficients $\alpha_v > 0$ and $\alpha_k > 0$ involved in the boundary conditions of (2.16) must be set. This point is discussed in section 4.1 below.*

3 Direct Numerical Simulations

We perform and validate in this section several DNS, in order to derive a universal formula for the mixing length ℓ as a function of the frictional Reynolds number

$$Re_\star = \frac{u^\star H}{\nu}, \tag{3.1}$$

the friction velocity $u_\star$ being given by (2.4), $H = L_z/2$. The frictional Reynolds number is the main control parameter in this study. To close the set of parameters, we enforce u to be equal to 1 at $z = H$. We will use the following standard relation between $u_\star$ and $Re_\star$:

$$u_\star = \left(\frac{1}{0.41} \log Re_\star + 5.5 \right)^{-1}, \tag{3.2}$$

which is a byproduct of the log law. Therefore, $Re_\star$ yields $u_\star$ and then ν from (3.1) re-written as

$$\frac{\nu}{u_\star} = \frac{H}{Re_\star}. \tag{3.3}$$

Note that $\nu/u_\star$ is the natural length scale of the flow.

3.1 Settings and results

To begin with, we set data and parameters for the simulations.

i) Software and equations. The direct numerical simulations (DNS) are performed by using the parallelised flow solver Incompact3d (see at https://www.incompact3d.com/). The numerical schemes implemented in this software are detailed in [16, 17, 19]. The equations, solved in $\Omega = [0, L_x] \times [0, L_y] \times [0, L_z]$, are[4]:

$$\begin{cases} \partial_t \mathbf{v} + \dfrac{1}{2}\left[\nabla \cdot (\mathbf{v} \otimes \mathbf{v}) + (\mathbf{v} \cdot \nabla)\mathbf{v}\right] - \nabla \cdot (\nu \nabla \mathbf{v}) + \nabla p = \mathbf{f}, \\ \nabla \cdot \mathbf{v} = 0, \\ \mathbf{v}|_{z=0} = \mathbf{v}|_{z=L_z} = 0, \quad \mathbf{v} \text{ periodic in the } x-y \text{ axes}, \\ \mathbf{v}|_{t=0} = \mathbf{v}_0. \end{cases} \tag{3.4}$$

The source term $\mathbf{f}$ is constant and given by

$$\mathbf{f} = \left(\frac{u_*^2}{H}, 0, 0\right). \tag{3.5}$$

ii) The initial data. The initial data $\mathbf{v}_0$ is a random perturbation of the field

$$\mathbf{U}(x, y, z) = \left(\left(\frac{\widetilde{z}}{H}\right)^{\frac{1}{7}}, 0, 0\right), \tag{3.6}$$

where $\widetilde{z} = \min(z, 2H - z)$. The corresponding profile coincides more or less with the log profile, without the singularity at $z = 0$ and $z = L_z$. In order to get a flow that is not too trivial and looks like a turbulent flow, we take $\mathbf{v}_0$ such that

$$\mathbf{v}_0 = \mathbf{U} + 0.125\eta(x, y, \widetilde{z}, \omega)\left(\left(\frac{\widetilde{z}}{H}\right)^{\frac{1}{7}}, 1, 1\right). \tag{3.7}$$

The function $\eta \in [-1, 1]$ is a zero mean Gaussian random variable: at each point (x, y, z) and each run labeled by ω, the code randomly picks a number $\eta(x, y, z, \omega)$, thanks to a standard numerical random generator. This field is not divergence free, but the code automatically correct this error at the first time step, through the incompressibility condition.

iii) Parameters of the simulations. They are the same as those of Moser et al [27], which is our benchmark. We have performed four DNS: three of them are in the flat case (see figure 2), for $Re_\star = 180, 360, 550$, and one in the rough case (see figure 1) for $Re_\star = 180$. Let Δt denotes the time step, T the final time of the simulation, (n_x, n_y, n_y) determines the mesh size, which means that the discretization space-step Δa in the a-axis ($a = x, y, z$) is given by

$$\Delta a = \frac{L_a}{n_a}.$$

Run	(L_x, L_y, L_z)	(n_x, n_y, n_z)	Δt	T
DNS-FLAT-180	$(4\pi, 4/3\pi, 2)$	$(128, 128, 128)$	0.005	$3600\nu/u_\star^2$
DNS-FLAT-360	$(2\pi, 2/3\pi, 2)$	$(256, 128, 192)$	0.0025	$3600\nu/u_\star^2$
DNS-FLAT-550	$(2\pi, 2/3\pi, 2)$	$(256, 256, 257)$	0.00125	$1800\nu/u_\star^2$
DNS-ROUGH -180	$(4\pi, 4/3\pi, 2)$	$(128, 128, 128)$	0.005	$3600\nu/u_\star^2$

Table 1: Parameters for each DNS

Since the Kolmogorov scale is getting smaller as $Re_\star$ increases, the computational cost is dramatically expensive for large $Re_\star$. This is why the dimensions of the computational boxes in DNS-FLAT-360 and 550 are smaller than the dimensions in DNS-FLAT-180.

iv) Results in the flat case.[5] Our results are reported in figure 3 where we have plotted the mean adimensionalized streamwise component of the velocity as well as the results of Moser et all [27]. In particular, if $\mathbf{v}_{\text{DNS}} = (u_{\text{DNS}}, v_{\text{DNS}}, w_{\text{DNS}})$ denotes the calculated field by the DNS,

$$\overline{u}(z) = \frac{1}{T n_x n_y} \sum_{n=0}^{T/\Delta t} \sum_{j=0}^{n_x} \sum_{k=0}^{n_y} u_{\text{DNS}} \left(n\Delta t, j\frac{L_x}{n_x}, k\frac{L_y}{n_y}, z \right). \tag{3.8}$$

We observe a very good correspondence between our results of those of [27], at least in

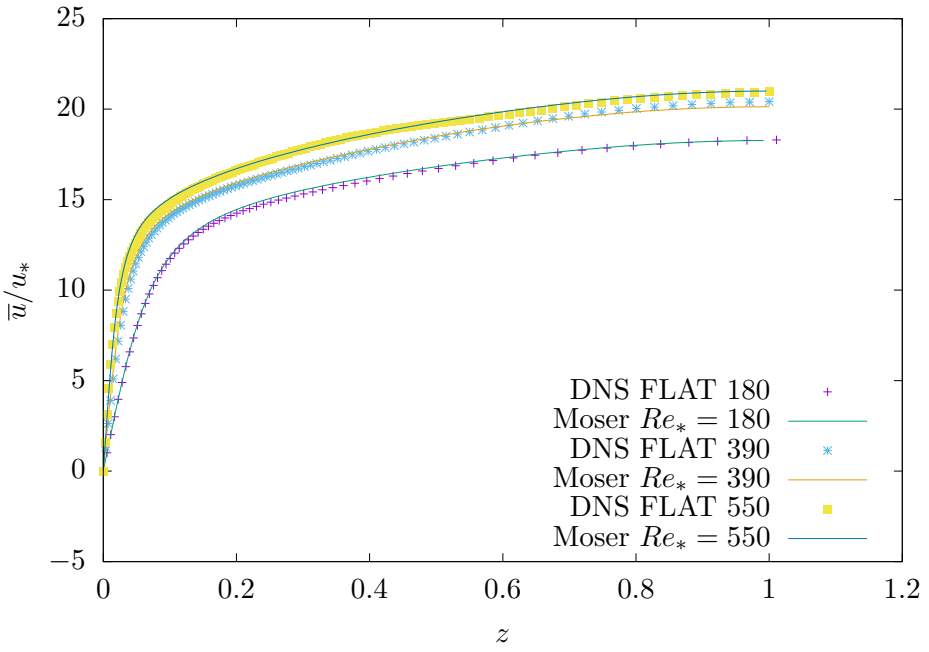

Figure 3: Streamwise velocity profile compared to those of [27].

average. This validates our DNS in the flat case, which allows us to think that our DNS in the rough case[6], outlined below, is accurate.

[4] numerically more convenient, theoretically equivalent to the standard Navier-Stokes equations

[5] For the simplicity, the overline always means an average which will be specified case by case, to avoid the risks of confusion. We also may use $\langle \cdot \rangle$ for time averages.

[6] So far we know, there is no available data in the literature for such a rough case.

v) The rough case. The rough topography displayed in figure 1 is built in three steps as follows.

1) We construct regularly spaced Gaussian domes centered at (x_i, y_i) with random heights $\tilde{\Lambda}_i$ and variances σ_i, leading to the primary topography $z = \tilde{\Lambda}(x, y)$ given by

$$\tilde{\Lambda}(x,y) = \sum_{i=1}^{N} \tilde{\Lambda}_i e^{-[(x-x_i)^2+(y-y_i)^2)]/(4\sigma_i^2)}. \tag{3.9}$$

2) This topography remains regular. In order to make it more chaotic, we follow [32] and we pick Gaussian domes Λ_j again, as well as random angles θ_j and aspect ratio a_j. Then we perturb $\tilde{\Lambda}(x, y)$ as follows:

$$\Lambda(x,y) = \tilde{\Lambda}(x,y) + \sum_{j=1}^{N} \Lambda_j e^{-[[c_j(x-x_j)+s_j(y-y_j)]^2/a_j^2+[c_j(y-y_j)-s_j(x-x_j)]^2 a_j^2]/(4\sigma_j^2))}, \tag{3.10}$$

where $c_j = \cos(\theta_j)$, $s_j = \sin(\theta_j)$, a_j. The Λ_j's, the θ_j'a and the a_j's are all Gaussian as well.

3) The roughness field is normalized such that $max(\Lambda(x, y)) = h_{max} = 0.1$. Therefore, the bottom is the surface given by: $z = \Lambda(x, y)$.

To perform the simulation, we use the "immersed boundary method" (IBM), initially developed by Peskin [30] (see also in [24]). This consists of solving the Navier-Stokes equation in $\Omega = [0, L_x] \times [0, L_y] \times [0, L_z]$, by adding in the Navier-Stokes equations (3.4) the additional source term

$$-\frac{1}{\varepsilon} \mathbb{1}_{\{0 \le z \le \Lambda(x,y)\}} \mathbf{v}, \tag{3.11}$$

for a small value of ε, which does not change the standard results and analysis about the Navier-Stokes equations[7]. This additional term enforces $\mathbf{v}$ to be negligible for $z \le \Lambda(x, y)$, and does not affect the system in the domain $\Lambda(x, y) \le z \le L_z$. The results of the simulation are reported in figure 4. We also have plotted on the same figure the log profile given by

$$h(z) = \frac{1}{0.31} \ln\left(\frac{z}{0.025}\right) + 7.0.$$

Our simulation yields a mean streamwise profile that perfectly matches with this log law for $z \in [0.3, 0.8]$, thereby validating our DNS.

3.2 Determination of the mixing length and the constants

The aim of this section is to derive from the DNS a formula to determine the mixing length ℓ. We also settle the values of the constants C_v and C_k involved in the boundary conditions at Γ_c for $\mathbf{v}$ and k.

[7] The comprehensive mathematical analysis of the IBM is carried out in [24].

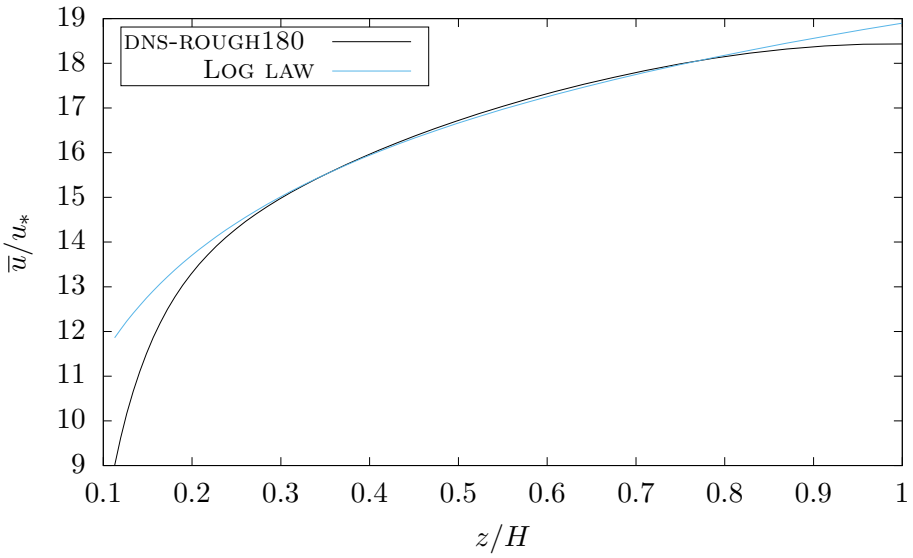

Figure 4: Streamwise velocity profile compared to a log profile.

3.2.1 General methodology

Let $\mathscr{E}$ denotes the total mean dissipation, given by

$$\mathscr{E} = 2\nu\overline{|\nabla \mathbf{v}|^2}. \tag{3.12}$$

It is common in turbulence modeling to assume that ℓ is a function of k and $\mathscr{E}$, that is $\ell = \ell(k, \mathscr{E})$. A straightforward dimensional analysis yields the formula

$$\ell = \frac{k\sqrt{|k|}}{\mathscr{E}}, \tag{3.13}$$

on which the determination of ℓ is based. We assume that ℓ does not depend on x and y. Therefore in this framework, the means are calculated from the data by the same formula as (3.8). To be more specific, if Ψ is any field related to the flow, Ψ_{DNS} the corresponding calculated field, then

$$\overline{\Psi}(z) = \frac{1}{Tn_xn_y}\sum_{n=0}^{T/\Delta t}\sum_{j=0}^{n_x}\sum_{k=0}^{n_y}\Psi_{\text{DNS}}\left(n\Delta t, j\frac{L_x}{n_x}, k\frac{L_y}{n_y}, z\right). \tag{3.14}$$

Of course, only numerical values of $\overline{\Psi}$ at $z = qL_z/n_z$ $(q = 0, \cdots, n_z)$ can be calculated by (3.14). Based on this, our procedure is the following:

i) we compute $\overline{\mathbf{v}} = \overline{\mathbf{v}}(z)$ by (3.14),

ii) at each grid point, we form the field $\mathbf{v}'_{vert} = \mathbf{v}_{\text{DNS}} - \overline{\mathbf{v}}$,

iii) we extract from the data the numerical TKE denoted by k_{vert}, given at each $z = qL_z/n_z$ by the quantity $k_{vert}(z) = (1/2)\overline{|\mathbf{v}'_{vert}|^2}(z)$,

iv) by the standard finite difference scheme, we calculate $\mathscr{E}_{vert} = \mathscr{E}_{vert}(z)$ by (3.12),

v) we get at each $z = qL_z/n_z$ the mixing length $\ell = \ell(z)$ by forming the quotient $k_{vert}(z)\sqrt{k_{vert}(z)}/\mathscr{E}_{vert}(z)$.

Remark 3.1. *The function $k_{vert}(z)$ calculated above is the horizontal mean of the TKE. This is the appropriate quantity for the determination of ℓ, according to the horizontal homogeneity assumption. To calculate the full TKE from the DNS, we must use the time average over the simulation time:*

$$\langle\psi\rangle(\mathbf{x}) = \frac{1}{T}\sum_{n=0}^{T/\Delta T}\psi_{DNS}(n\Delta T, \mathbf{x}), \tag{3.15}$$

where $\mathbf{x} = (x, y, z)$. Then the Reynolds decomposition is written as $\mathbf{v}_{DNS} = \langle\mathbf{v}\rangle + \mathbf{v}'_{DNS}$, yielding

$$k_{DNS}(\mathbf{x}) = (1/2)\langle|\mathbf{v}'_{DNS}|^2\rangle. \tag{3.16}$$

We have plotted in figure 5 the curves of ℓ we have obtained by this way, in terms of the non dimensional variable $z' = z/H$.

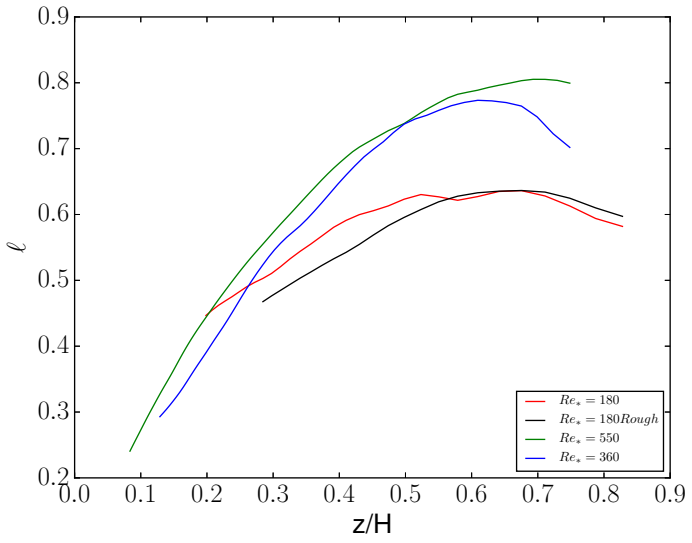

Figure 5: Profils of ℓ calculated from the DNS

3.2.2 Universal formula for the mixing length

We observe that the mixing length is increasing in the beginning of the turbulent layer (until $z \approx 0.6$) and slighly decreases until $z = 1$. Our goal is to interpolate these curves to get a universal formula in terms of the $Re_\star$ and z, by an empirical method.
Figure 5 suggests to seek for exponential profils. However, it is usually accepted that near $z = 0$, ℓ is of the form $\ell = \kappa z$. Therefore, we multiply this exponential profile by an hyperbolic tangent function, which is an approximation of the Heaviside function. Finally, since ℓ is non-zero within the viscous sublayer, we add a term that depends on the natural length scale $\nu/u_\star = H/Re_\star$. These considerations have led us to introduce the following empirical formula by trial and error:

$$\ell = K\tanh\left(A\left(Re_\star\frac{z}{H} - B\right)\right)\exp\left(-Re_\star^2\frac{\left(\frac{z}{H} - \frac{z_i}{H}\right)^2}{2\sigma}\right) + 75\frac{H}{Re_\star} \tag{3.17}$$

where $z_i = 0.6H\,m$. In the rough case, by comparing the red line to the dark line in figure 5 (DNS-FLAT 180 and DNS-ROUGH 180) we apply a correction that takes the topography into account, which gives:

$$\ell = K \tanh\left(A\left(Re_\star \frac{z+z_R}{H} - B\right)\right) \exp\left(-Re_\star^2 \frac{\left(\frac{z+z_R}{H} - \frac{z_i}{H}\right)^2}{2\sigma}\right) + 75\frac{H}{Re_\star} \tag{3.18}$$

where $z_R = 0.05H\,m$ is the mean value of the roughness, estimated from Figure 5. It remains to settle the coefficients A, B, σ and K. They are sought to be function of $Re_\star$ only. As we shall show it in the following, we get the following laws for large values of $Re_\star$ (valid from $Re_\star = 900$, depending on the coefficients):

$$A = 3.05 Re_*^{0.065}, \tag{3.19}$$

$$B = 0, \tag{3.20}$$

$$\sigma = 0.3 Re_*^{1.05}, \tag{3.21}$$

$$K = 0.32 Re_*^{0.12}. \tag{3.22}$$

Moreover, it is accepted that near $z = 0$, $\ell = \kappa z$ where κ is the von Kármán constant. However, according to figure 7, although ℓ follows well a linear law near $z = 0$, its slope looks non constant when $Re_\star$ varies. Indeed, we obtain from our graphs (see Figure 12 below) the following law, valid from $Re_\star \approx 800$:

$$\kappa = \kappa(Re_\star) = 0.25(Re_\star)^{0.32} \quad \text{hence} \quad \ell = 0.25(Re_\star)^{0.32} z. \tag{3.23}$$

However, we observe in Figure 12 that the usual law is valid for instance when $Re_\star = 180$. The law (3.17) must be checked for high values of $Re_\star$, which is done by applying the

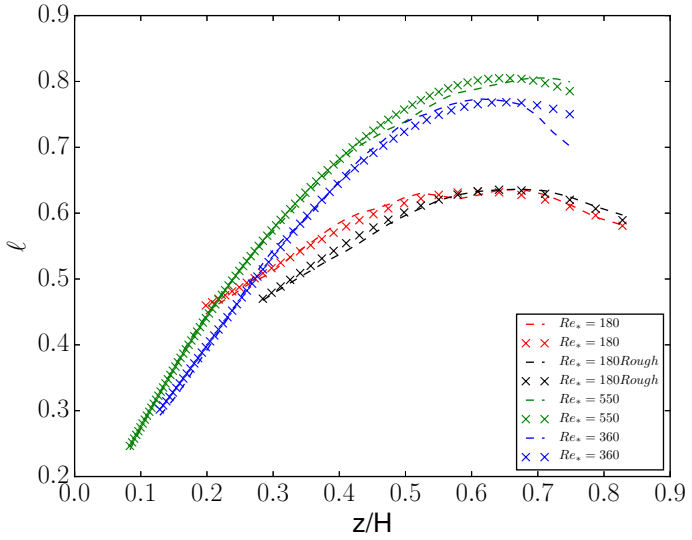

Figure 6: Dotted lines draw the mixing length calculated from the DNS, Crosses draw curves from formula (3.17) and (3.18)

algorithm to the results of Moser and al in Figure 7, and also yields the laws satisfied by the coefficients A, B, σ and K for high values of $Re_\star$, also used in the rough case.
In Figures 8 and 9, we have plotted the values of the constants A and B.
Figure 10 shows that the coefficient σ follows a linear law for all $Re_\star$, hence (3.19).

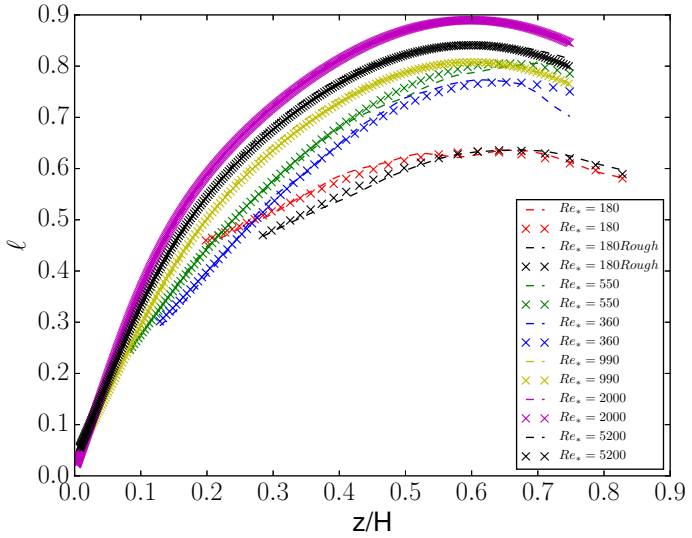

Figure 7: Lines are results from Moser and al [27], Crosses results from formulae (3.17) and (3.18)

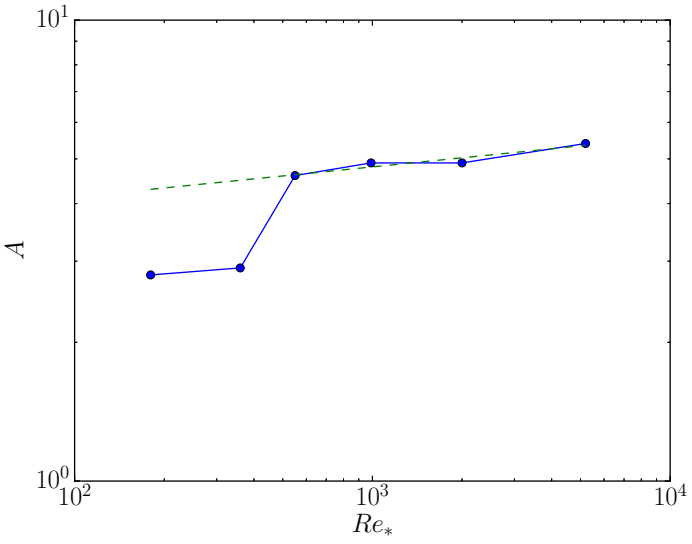

Figure 8: $A = A(Re_\star)$. The green dotted line is the 0.065 slope.

3.2.3 Determination of the constants

We recall that the eddy viscosities/diffusion ν_t and μ_t are given by

$$\nu_t(k) = C_v \ell \sqrt{k}, \quad \mu_t(k) = C_k \ell \sqrt{k}.$$

Now that we know how to compute ℓ thanks to (3.17), we are able to estimate the constants C_v and C_k as follows. In this section, $\langle \psi \rangle$ denotes the time average over the time simulation defined by (3.15), and the TKE k in the formulae below is given by (3.16). Because of the horizontal homogeneity assumption, we focus on the vertical components of the Reynolds

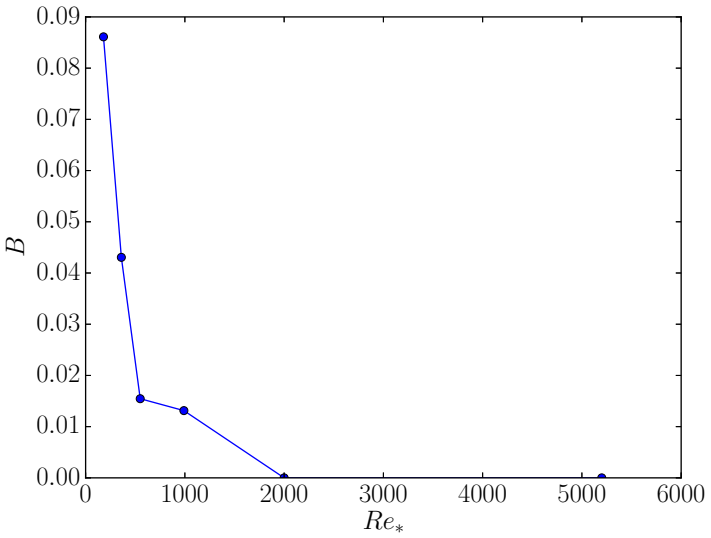

Figure 9: $B = B(Re_\star)$

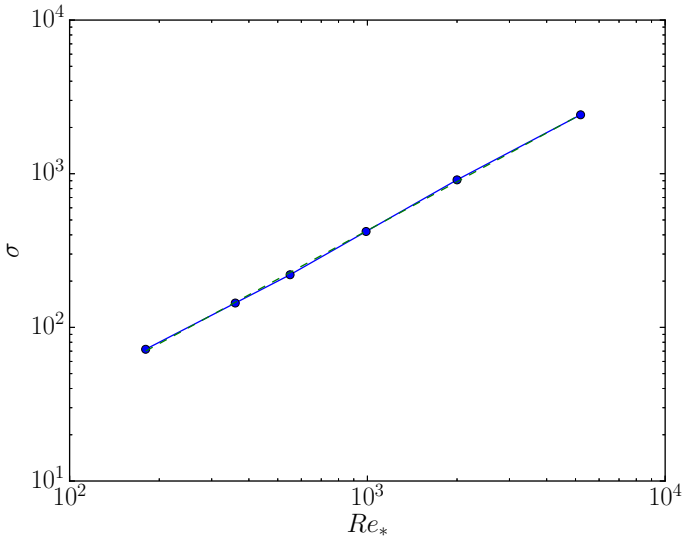

Figure 10: $\sigma = \sigma(Re_\star)$. The green doted line is the 1.05 slope.

stress, linked to the eddy coefficients by:

$$\langle u'_{\mathrm{DNS}} w'_{\mathrm{DNS}} \rangle = \nu_t \frac{\partial \langle u_{\mathrm{DNS}} \rangle}{\partial z} = C_v \ell \sqrt{k_{\mathrm{DNS}}} \frac{\partial \langle u_{\mathrm{DNS}} \rangle}{\partial z}, \tag{3.24}$$

and

$$\langle e'_{\mathrm{DNS}} w'_{\mathrm{DNS}} \rangle = \mu_t \frac{\partial k_{\mathrm{DNS}}}{\partial z} = C_k \ell \sqrt{k_{\mathrm{DNS}}} \frac{\partial k_{\mathrm{DNS}}}{\partial z}. \tag{3.25}$$

Hence, C_v is the value that minimizes the error in (3.24) whereas C_k is the value that minimizes the error in (3.25). By the least square method, C_v is such that

$$\sum_{i=1}^{N} \left(\langle u'_{\mathrm{DNS}} w'_{\mathrm{DNS}} \rangle (\mathbf{x}_i) - C_v \ell(z_i) \sqrt{k_{\mathrm{DNS}}(\mathbf{x}_i)} \frac{\partial \langle u_{\mathrm{DNS}} \rangle}{\partial z} (\mathbf{x}_i) \right)^2 \tag{3.26}$$

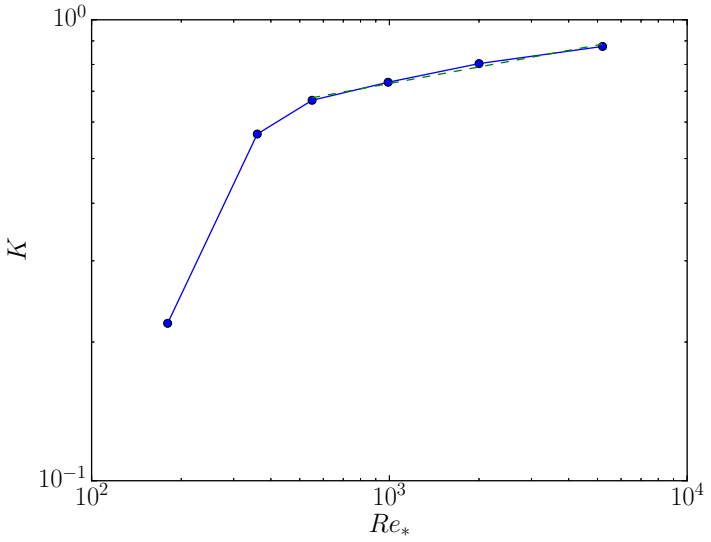

Figure 11: $K = K(Re_\star)$. The green dotted line is the 0.12 slope.

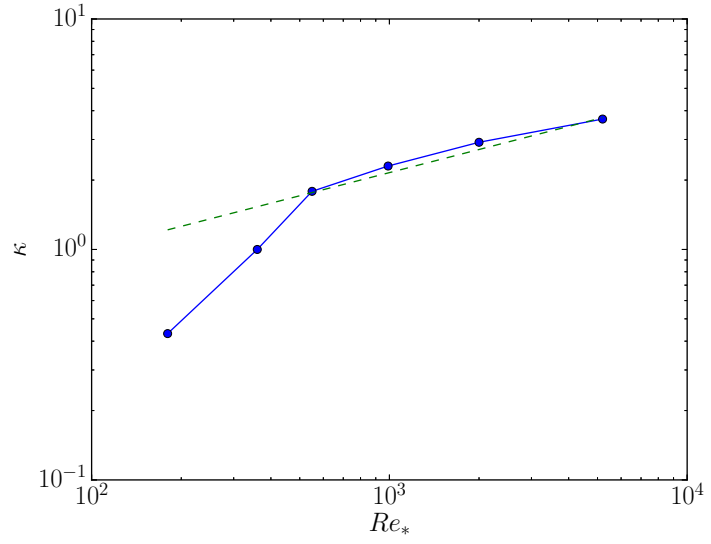

Figure 12: $\kappa = \kappa(Re_\star)$. The green dotted line is the 0.32 slope.

is minimum, and C_k is such that

$$\sum_{i=1}^{N}\left(\langle e'_{\rm DNS}w'_{\rm DNS}\rangle(\mathbf{x}_i) - C_k\ell(z_i)\sqrt{k_{\rm DNS}(\mathbf{x}_i)}\frac{\partial k_{\rm DNS}}{\partial z}(\mathbf{x}_i)\right)^2 \tag{3.27}$$

is minimum, where $\{\mathbf{x}_1,\cdots,\mathbf{x}_N\}$ denotes the grid points set, $\mathbf{x}_i=(x_i,y_i,z_i)$. This optimization problem has been solved by the *brute-force* method [2], based on the results of DNS-FLAT 180, DNS-FLAT 550 and the corresponding profiles for ℓ. We get:

$$C_k = 0.15 \quad C_v = 0.105 \tag{3.28}$$

Remark 3.2. *We find in [25, Chapter 4]: $C_v = C_k = 0.09$. However, these values have been calibrated for the full $k-\mathscr{E}$ model, which can explain the slight difference with our results.*

4 NSTKE simulations and conclusions

4.1 Algorithm and settings

Our code is based on the SIMPLEC algorithm (Patankar [28], Issa [15]), that we have adapted to the NSTKE equations, leading to encode the following iterations. At step n, $(\mathbf{v}^{n-1},p^{n-1},k^{n-1})$ being known, we first solve the velocity equation

$$\left\{\begin{array}{rcll}
(\overline{\mathbf{v}}^{n-1}\cdot\nabla)\,\overline{\mathbf{v}}^n - \nabla\cdot\left[(2\nu+\nu_t(k^{n-1}))\,D\overline{\mathbf{v}}^n\right] + \nabla p^{n-1} &=& \mathbf{f} & \text{in Om}_c,\\
\nabla\cdot\overline{\mathbf{v}}^n &=& 0 & \text{in Om}_c,\\
-[(2\nu+\nu_t(k^{n-1}))D\overline{\mathbf{v}}^n\cdot\mathbf{n}]_\tau &=& \alpha_v|\overline{\mathbf{v}}^{n-1}|\overline{\mathbf{v}}^n & \text{on } G_c,\\
\overline{\mathbf{v}}^n\cdot\mathbf{n} &=& 0 & \text{on } G_c,
\end{array}\right. \tag{4.1}$$

which is a standard elliptic equation, with the added difficulties presented by the incompressibility constrain and the boundary condition $\overline{\mathbf{v}}^n\cdot\mathbf{n}|_{G_c}=0$. Once $\mathbf{v}^n$ is calculated, we solve the TKE equation:

$$\left\{\begin{array}{rcll}
\overline{\mathbf{v}}^n\cdot\nabla k^n - \nabla\cdot[(\mu+\mu_t(k^{n-1})\nabla k^n] &=& \nu_t(k^{n-1})|D\overline{\mathbf{v}}^n|^2 - \dfrac{k^n\sqrt{|k|^{n-1}}}{\ell} & \text{in Om}_c,\\
-(\mu+\mu_t(k^{n-1}))\dfrac{\partial k^n}{\partial\mathbf{n}} &=& \alpha_k k^n\sqrt{|k|^{n-1}} & \text{on } G_c.
\end{array}\right. \tag{4.2}$$

Finally, the pressure is calculated by the Poisson equation:

$$\left\{\begin{array}{rcll}
\Delta p^n &=& -\nabla\cdot\left(\nabla\cdot(\mathbf{v}^n\otimes\mathbf{v}^{n-1}) - \nabla\cdot\left[(2\nu+\nu_t(k^{n-1}))\,D\mathbf{v}^n\right] - \mathbf{f}\right) & \text{in Om}_c,\\
\dfrac{\partial p^n}{\partial\mathbf{n}} &=& 0 & \text{on } G_c.
\end{array}\right. \tag{4.3}$$

System (4.1)-(4.2)-(4.3) for a given n, satisfies periodic boundary conditions in the $x-y$ axes. The source term $\mathbf{f}$ is given by (3.5). We implement this scheme in the OpenFoam solver (see at https://www.openfoam.com), based on the second order finite volumes method (see in [13]).

Remark 4.1. *Although we observe a good numerical convergence (see section 4.2.3 below), we have no mathematical proof of the convergence of this scheme to the NSTKE model, which is a difficult open question. Usually, we know that such scheme does converge when the eddy viscosity is close to a constant and when the source term is small enough in some sense (see in [21]). However, it is likely that the homogeneous Neumann boundary condition for the pressure in the equation (4.3) may yield serious complications in a mathematical convergence analysis.*

We have carried out four simulations in the flat case for high Reynolds numbers, namely $Re_\star = 990, 2000, 5200, 10000$. Then we have tested the rough case for $Re_\star = 5200, 10000$. The mixing length is given by (3.17) (flat case) and (3.18) (rough case), the constants C_v and C_k by (3.28). The iterations (4.1)-(4.2)-(4.3) are initialized by

$$\mathbf{v}^0 = (u^0, 0, 0), \quad u^0 = 1\, ms^{-1}; \quad k^0 = 10^{-3}\, m^2 s^{-2}; \quad p^0 = 0\, Pa. \tag{4.4}$$

The parameter settings are given in Table 2. The coefficients α_v and α_k have been determined up to $Re_\star = 5000$ by solving the minimization problem

Run	(L_x, L_y, L_z)	(n_x, n_y, n_z)	α_v	α_k
NSTKE-FLAT-990	$(6.28, 4.18, 2)$	$(16, 16, 32)$	0.000125	0.04
NSTKE-FLAT-2000	$(6.28, 4.18, 2)$	$(16, 16, 32)$	0.0000525	0.01
NSTKE-FLAT-5200	$(6.28, 4.18, 2)$	$(16, 16, 32)$	0.000035	0.0005
NSTKE-FLAT-10000	$(6.28, 4.18, 2)$	$(16, 16, 64)$	0.000035	0.0005
NSTKE-ROUGH-5200	$(6.28, 4.18, 2)$	$(32, 24, 64)$	0.000035	0.0005
NSTKE-ROUGH-10000	$(6.28, 4.18, 2)$	$(32, 24, 64)$	0.00035	0.0005

Table 2: Parameters settings

$$\min\{||\mathbf{v}_{\text{NSTKE}} - \mathbf{v}_{\text{DNS}}||_2^2 + ||k_{\text{NSTKE}} - k_{\text{DNS}}||_2^2\}. \tag{4.5}$$

The resolution of problem (4.5) is based on a standard dichotomy algorithm (see for instance in [37]). We have kept the same values for $Re_\star = 10000$, in the flat case as well as in the rough case, in the absence of DNS. Notice that the mesh sizes in this case are much more coarser than those used for the DNS, which is an undeniable advantage of the model. However, considering that the height of the viscous sublayer is negligible compared to this resolution, we have taken $z_0 = 0$ in the simulations for the flat case. The number of iterations is of order 1000.

4.2 Numerical Results in the flat case

4.2.1 Streamwise velocity

The results we get are compared to those of the high Reynolds numbers DNS provided in [18], up to $Re_\star = 5200$. For $Re_\star = 10000$, we have compared our result to the log law, in the absence of anything better. The NSTKE model yields a departure from the log law. However, things seem better when $Re_\star$ increases, which may be only a trend reversal near the bottom. To corroborate these observations, we have calculated the non dimensional mean shear defined by

$$\Phi = \frac{\kappa z}{u_*} \frac{\partial \overline{u}}{\partial z}, \tag{4.6}$$

which is equal to 1 when the profile is logarithmic. The results are plotted in Figure 14. The streamwise velocity given by the NSTKE model has a serious lack of shear at the top and the bottom of the boundary layer.

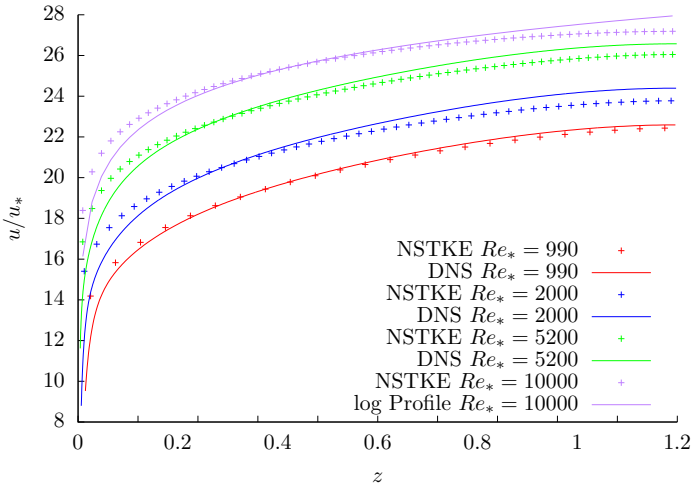

Figure 13: NSTKE Flat case. Non dimensional streamwise velocity

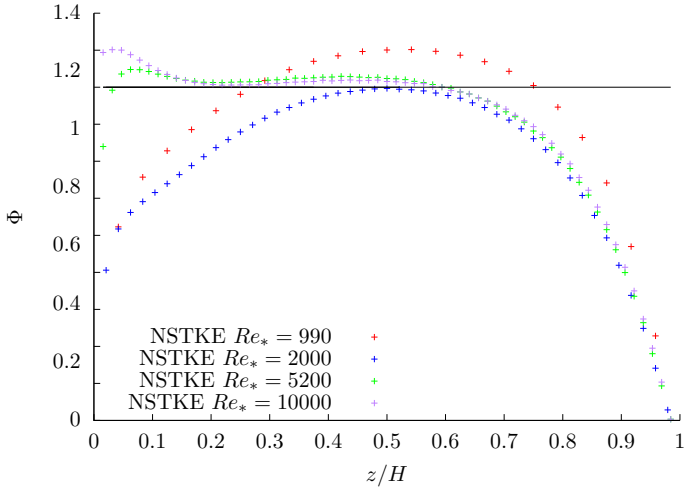

Figure 14: NSTKE Flat case. Comparison of the non dimensional mean shear Φ computed by the NSTKE model for the High Reynolds number simulations.

4.2.2 Turbulent kinetic energy

The turbulent kinetic energy is plotted on Figure 15, compared with the DNS results.The model overestimates the TKE at the bottom of the boundary layer.

4.2.3 Convergergence analysis

The convergence of the SIMPLEC algorithm for the NSTKE problem is shown in figure 16 for the $Re_\star = 900, 2000, 5200$ cases. The black lines indicates the slope of the decreasing rate, which is proportional to $n^{-2/3}$ for the first 300 iterations and increases up to n^{-8} until $n = 1000$, which is a good convergence result.

4.2.4 Corrected mixing length

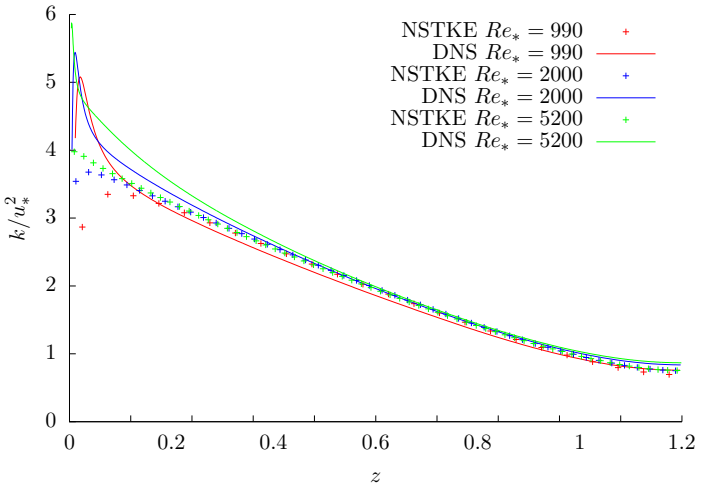

Figure 15: NSTKE Flat case. Turbulent kinetic energy

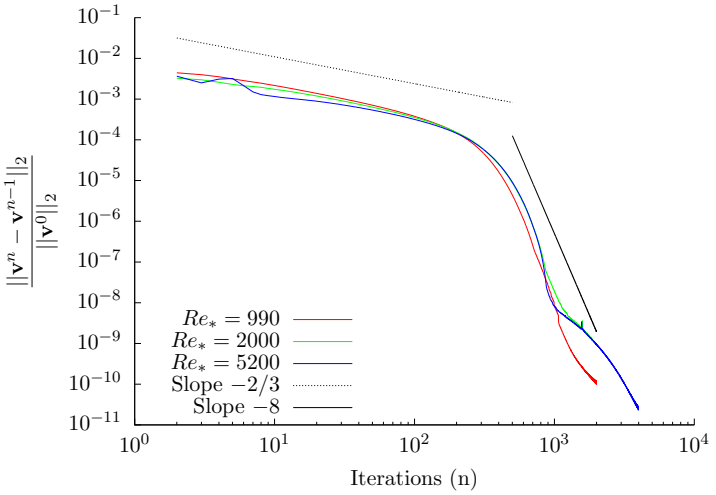

Figure 16: Convergence analysis.

The previous sections show that the NSTKE model does not perfectly reproduce the standard boundary layer profiles. It may come from the mixing length formula (3.17) and the law (3.19) that determines the main coefficient in the formula for ℓ, denoted by A. To fix this issue, we have replaced A by another coefficient of the form λA, the best choice of λ being equal to 0.608, after some simulations. As shown by the figure (17), the corrected model accurately reproduces the log profile up to $z = 0.7H$, which is quite satisfactory. About the TKE, it does not change much, in particular at high Reynolds number.

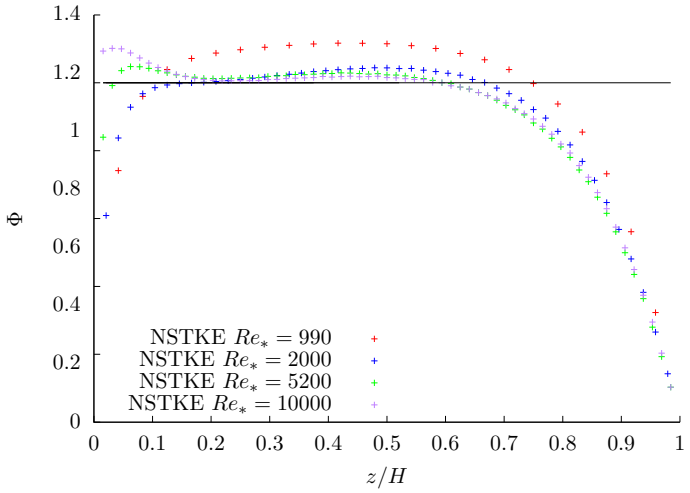

Figure 17: NSTKE Flat case. Mean shear Φ with the corrected mixing length profile.

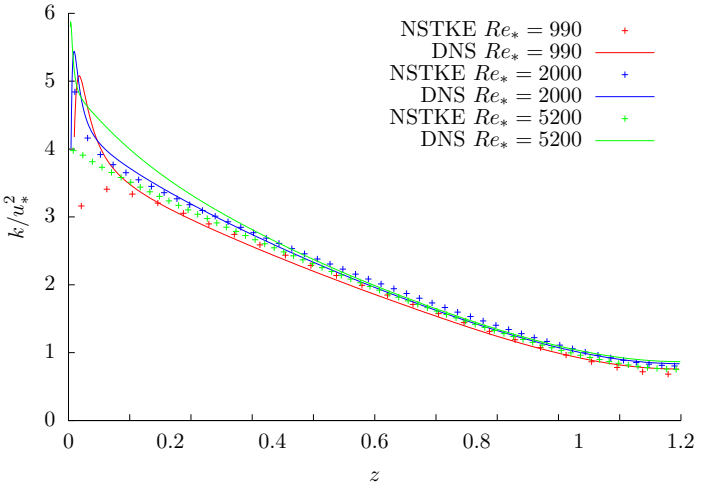

Figure 18: NSTKE Flat case. Turbulent kinetic energy with the corrected mixing length profile.

4.3 Numerical results in the rough case

The simulation is carried out from $z_0 = 0.1$. This is as if we have put a flat plate over the domes, starting the simulation from z_0 as in the flat case, the information about the topography being contained in the formula for ℓ, the boundary condition and the corresponding coefficients. We have applied the same correction for the coefficient A in

formula (3.18) as in the flat case (see section 4.2.4 above). The results are reported in Figure 19, Figure 20 and Figure 21, following the same order as in the flat case. Without any DNS, the only way to analyse the results is the comparison with log profiles. We observe a departure from the log law outside the interval $[0.5, 0.7]$. Considering the TKE profiles, the intensity of the turbulence for $Re_\star = 5000$ and $Re_\star = 5000$ looks to be different only from $z/H = 0.5$.

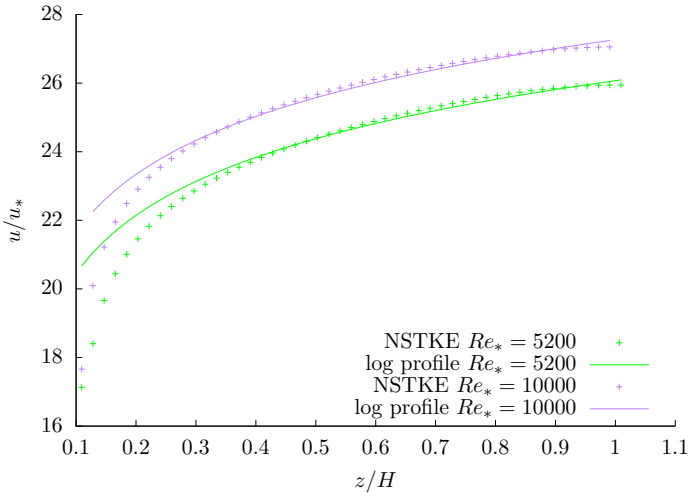

Figure 19: NSTKE Rough case. Non dimensional streamwise velocity.

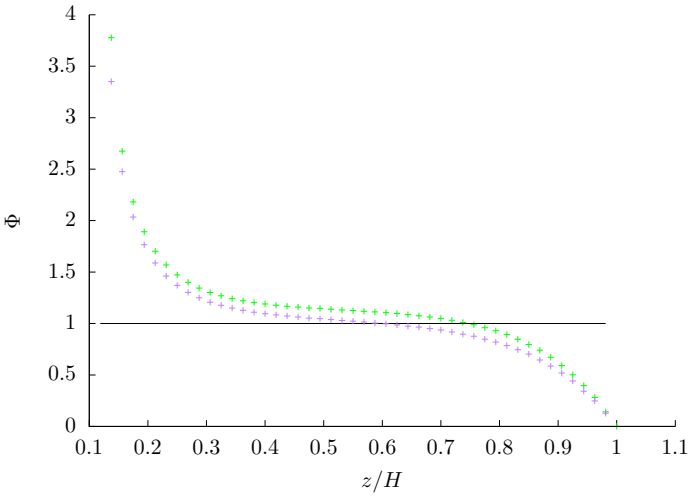

Figure 20: NSTKE Rough case. Mean shear

4.4 Some conclusions and perspectives

The NSTKE model yields satisfactory results in the flat case, although we had to adjust the formula calculated from the DNS for ℓ. The treatment of the pressure in the SIMPLEC algorithm could be questionable, in particular because of the boundary condition (4.3). Further simulation are probably necessary with another treatment of the pressure, following what was done in [11, Chapters 13], where similar simulations for low Reynolds

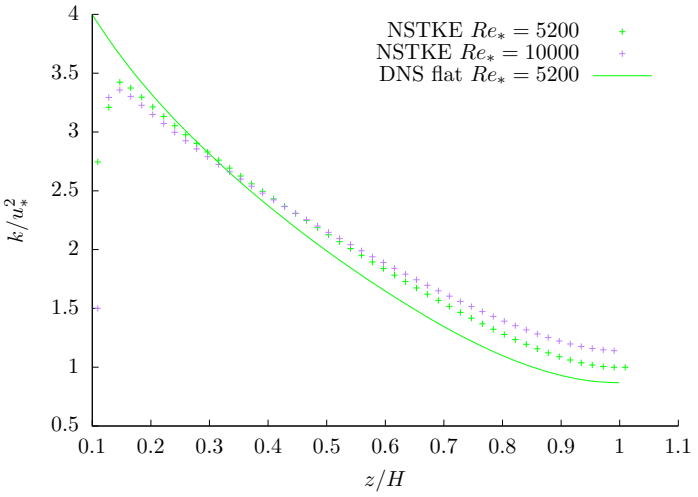

Figure 21: NSTKE Rough case. Turbulent kinetic energy

numbers are performed by the variational multi-scale method and a perturbation of the incompressibility constrain to resolve the pressure.
In the rough case, the present study cannot be considered as fully conclusive, but as a first step towards a general methodology to tackle this class of difficult numerical problems. These simulations suggest that the topography must be taken into account for the determination of the coefficients α_v et α_k in the boundary conditions (1.2) and (2.12), which has not been done already. The question is how to do that? Moreover, it is likely that ℓ does not depend on z only, but also on x, y in a way that depends on the topography. To fix this, several other DNS are necessary in the rough case, for the highest possible $Re_\star$, expecting for a generic formula for $\ell(x, y, z, Re_\star)$, as well as $\alpha_a(x, y, z, Re_\star)$ $(a = v, k)$. This will be the subject of a next study.

Appendices

A Theoretical analysis of the NSTKE model

We aim to prove the existence of a weak solution $(\overline{\mathbf{v}}, p, k)$ to the boundary value problem (2.16). Standard à priori estimates yield $\nu_t(k)|D\overline{\mathbf{v}}|^2 \in L^1(\Omega)$, so that (2.16) couples a steady-state Navier-Stokes like equation to an elliptic equation with a right hand side in L^1.
Throughout this theoretical appendix, the mixing length $\ell = \ell(\mathbf{x})$ is a given strictly non negative bounded continuous function, $\nu > 0$, $\mu > 0$, $\alpha_v > 0$, $\alpha_k > 0$ are constants, the eddy viscosity $\nu_t = \nu_t(k) \geq 0$ and $\mu_t = \mu_t(k) \geq 0$ are continuous function of k.

A.1 Brief state of the art

The NSTKE model was first studied in [23], where $\Omega \subset \mathbb{R}^d$ $(d = 2, 3)$ is a smooth bounded domain, with homogeneous boundary condition in the whole boundary of Ω, that is $\overline{\mathbf{v}}|_{\partial\Omega} = 0$ and $k|_{\partial\Omega} = 0$, and where ν_t and μ_t are bounded continuous functions of k. Steady state and evolutionary cases were considered in this paper, in which various existence and stability results are proved.

In [10], the model was studied in $\Omega \subset \mathbb{R}^3$, $\overline{\mathbf{v}}$ satisfies the (linear) Navier Law at $\partial\Omega$, k satisfies mixed homogeneous Dirichlet/Neumann boundary condition at $\partial\Omega$, ν_t and μ_t are continuous functions of k, with growth condition at infinity, covering the case $\nu_t, \mu_t = O\left(k^{1/2}\right)$. In this paper, the k-equation is replaced by the equation for the total energy $e = 1/2|\overline{\mathbf{v}}|^2 + k$, and the existence of a weak solution to the $(\overline{\mathbf{v}}, p, e)$ system is proved.
In [11], we have studied the NSTKE model in $\Omega \subset \mathbb{R}^3$ with the boundary conditions (1.2) (wall law) and (1.3) ($k_{\partial\Omega} = |\overline{\mathbf{v}}|^2$) at the whole boundary. To carry out this study, we have set $k' = k - |\overline{\mathbf{v}}|^2$ and considered the equation for k' in place of that for k. The advantage is that k' satisfies an homogeneous Dirichlet boundary conditions at $\partial\Omega$, suggesting that the method developed in [23] might be adapted. The disadvantage is that additional coupling terms appear in the equation for k'.
In the steady state case, we have proved in [11, Chapters 7] the existence of a weak solution to the $(\overline{\mathbf{v}}, \overline{p}, k')$ system when $\nu_t = \nu_t(k)$ and $\mu_t = \mu_t(k)$ are continuous bounded function of k, by a very long and technical proof. When $\nu_t, \mu_t = O\left(k^{1/2}\right)$ at infinity, we still get an existence result when the equality in the k' equation is replaced by a variational inequality. The method fails in the evolutionary case, which still remains an open problem. In this evolutionary case, we have been able to obtain existence results when $k|_{\partial\Omega} = 0$ and $\overline{\mathbf{v}}$ satisfies the wall law (1.2).
In comparison with the former studies, the boundary value problem (2.16) is characterized by

i) mixed boundary conditions, in the sense that they are periodic in the $x - y$ axes, and of flux type in the z-axis (wall law, Neumann),

ii) the non linear Neumann boundary condition (2.13) for k in the z axis.

In what follows, we will limit ourselves to focus on these special features, to avoid repeating arguments already written in former works. In particular, it will be enough to carefully detail the functional setting, and to study the Laplace equation with a right hand side in L^1, periodic boundary conditions in the (x, y)-axes, and (2.13) in the z-axis, which was not already carried out elsewhere, up to our knowledge.

A.2 Functional spaces

This section is devoted to define the functional spaces we are working with, which will be done step by step. Let us first set

$$\Omega_c = [0, L_x] \times [0, L_y] \times [z_0, L_z - z_0], \tag{A.1}$$

$$\Gamma_{b,c} = [0, L_x] \times [0, L_y] \times \{z = z_0\} \quad \text{(bottom)}, \tag{A.2}$$

$$\Gamma_{t,c} = [0, L_x] \times [0, L_y] \times \{z = L_z - z_0\} \quad \text{(top)}, \tag{A.3}$$

$$\Gamma_c = \Gamma_{b,c} \cup \Gamma_{t,c}. \tag{A.4}$$

i) Suitable space for the periodic boundary conditions in the (x, y)-axes. It is natural to introduce the following functional space:

(A.5)
$$\mathcal{W} = \left\{\psi \in C^\infty(\mathbb{R}^2 \times [z_0, L_z - z_0], \mathbb{R}) \text{ s.t.} \right.$$
$$\left. \forall\, (m, n) \in \mathbb{N}^2,\ \forall\, (x, y, z) \in \Omega_c,\ \psi(x + nL_x, y + mL_y, z) = \psi(x, y, z)\right\},$$

that means the smooth function defined in the strip $z_0 \leq z \leq L_z - z_0$, periodic in the (x, y)-axes by the $[0, L_x] \times [0, L_y]$ box. Given any $\psi \in \mathcal{W}$, we still denote by ψ its restriction to Ω_c, so far no risk of confusion occurs.

Let us consider on $\mathcal{W}$ the following norm:

$$||\psi||_{1,2} = \left(\int_{\Omega_c} |\nabla\psi|^2\right)^{\frac{1}{2}} + \left(\int_{\Omega_c} |\psi|^2\right)^{\frac{1}{2}} = ||\psi||_{1,2,\Omega_c}. \tag{A.6}$$

Generally speaking, for any $s \geq 0$, $1 \leq p \leq \infty$, we set

$$||\psi||_{s,p} = ||\psi||_{s,p,\Omega_c}, \tag{A.7}$$

where $||\psi||_{s,p,\Omega_c}$ denotes the $W^{s,p}$ norm of the restriction of ψ to Ω_c. Due to the periodicity in the (x, y)-axes, these are norms on $\mathcal{W}$. We denote by $W^{s,p}_\pi$ the completion of $\mathcal{W}$ with respect to the $||\cdot||_{s,p}$ norm.

Remark A.1. *Let $W^{s,p}_\pi|_{\Omega_c}$ be the space of the restrictions to Ω_c of functions of $W^{s,p}_\pi$. Then $W^{s,p}_\pi|_{\Omega_c}$ is a closed subspace of $W^{s,p}(\Omega_c)$.*

We will write in the remainder:

$$H^1_\pi = W^{1,2}_\pi, \quad L^p_\pi = W^{0,p}_\pi. \tag{A.8}$$

ii) Vertical homogeneous space. We will need the following space:

$$\begin{aligned} \mathcal{W}_0 = \{&\psi \in \mathcal{W} \text{ s.t.} \\ &\exists\, \delta > 0,\ \forall\, (x, y) \in \mathbb{R}^2,\ \forall z \in [z_0, z_0 + \delta] \cup [L_z - z_0 - \delta, L_z - z_0], \\ &\psi(x, y, z) = 0\}. \end{aligned} \tag{A.9}$$

In other word, $\mathcal{W}_0$ is the set of functions in $\mathcal{W}$ vanishing in a neighbourhood of the bottom $z = z_0$ and the top $z = L_z - z_0$. We denote by $W^{1,p}_{\pi,0}$ the adherence of $\mathcal{W}_0$ in $W^{1,p}_\pi$. It easy checked that given any $\psi \in W^{1,p}_\pi$, then $\psi \in W^{1,p}_{\pi,0}$ if and only if $\psi|_{\Gamma_c} = 0$ (see [9]). Moreover, the following Poincaré's inequality holds

$$\forall\, \psi \in W^{1,p}_{\pi,0}, \quad ||\psi||_{0,p,\Omega_c} \leq C_{p,\Omega_c} ||\nabla\psi||_{0,p,\Omega_c}, \tag{A.10}$$

where C_{p,Ω_c} is a constant that only depends on p and Ω_c. Note that in view of the geometry of Ω_c, a straightforward calculation using Fubini's theorem allows to check that (A.10) can be improved by:

$$\forall\, \psi \in W^{1,p}_{\pi,0}, \quad ||\psi||_{0,p,\Omega_c} \leq C_{p,L_z} ||\frac{\partial\psi}{\partial z}||_{0,p,\Omega_c}, \tag{A.11}$$

iii) Norm with the trace. Because of the boundary conditions involved in problem (2.16), it is convenient to consider norms on $W^{1,p}_\pi$ that take the traces on Γ_c into account. The general framework is the following:

- Given any $1 \leq p < 3$, $p^\star = \dfrac{3p}{3-p}$ is the critical exponent for the space $W^{1,p}(\Omega_c)$,
- For all $\psi \in W^{1,p}_\pi$, $\mathrm{tr}_b\psi$ (resp. $\mathrm{tr}_t\psi$) denotes the trace of ψ at the bottom $\Gamma_{b,c}$ (resp. at the top $\Gamma_{t,c}$). In this case, according to the theory of traces (see in [1]) $\mathrm{tr}_\alpha\psi \in W^{1-1/p,p}(\Gamma_{\alpha,c})$ for $\alpha =$ b,t. Because of the Sobolev embedding theorem, $\mathrm{tr}\psi \in L^q(\Gamma_c)$ for any

  $$1 \leq q \leq \frac{2p}{3-p} = p^{\star\star}, \tag{A.12}$$

  where $\mathrm{tr}\psi(\mathbf{x}) = \mathrm{tr}_\alpha\psi(\mathbf{x})$ if $\mathbf{x} \in \Gamma_{\alpha,c}$, for $\alpha =$ b,t.

Lemma A.1. *Let $1 \leq p < 3$, $1 \leq q < p^{\star\star}$. Then the application*

$$N_{p,q} : \begin{cases} W^{1,p}_{\pi} \longrightarrow \mathbb{R}_+, \\ \psi \longrightarrow ||\nabla\psi||_{0,p,\Omega_c} + ||\mathrm{tr}\psi||_{0,q,\Gamma_c}, \end{cases} \tag{A.13}$$

is a norm on $W^{1,p}_{\pi}$, equivalent to the standard $W^{1,p}$-norm.

Proof. The application $N_{p,q}$ is obviously a semi norm. To check that it is a norm, let us consider $\psi \in W^{1,p}_{\pi}$ such that $N_{p,q}(\psi) = 0$. In particular $\psi|_{\Gamma_c} = 0$. Therefore, $\psi \in W^{1,p}_{\pi,0}$, hence as $||\nabla\psi||_{0,p,\Omega_c} = 0$, we get from Poincaré's inequality, $||\psi||_{0,p,\Omega_c} = 0$. Then $\psi|_{\Omega_c} = 0$, and by periodicity, $\psi = 0$.
To prove that $N_{p,q}$ is equivalent to the $W^{1,p}$ norm, it is enough to prove that there exists a constant C such that

$$\forall\, \psi \in W^{1,p}_{\pi}, \quad ||\psi||_{0,p,\Omega_c} \leq C N_{p,q}(\psi). \tag{A.14}$$

If (A.14) would not hold true, there would be a sequence $(\psi_n)_{n\in\mathbf{N}}$ in $W^{1,p}_{\pi}$ such that $||\psi_n||_{0,p,\Omega_c} = 1$ and $N_{p,q}(\psi_n) \to 0$ as $n \to \infty$. Such a sequence is bounded in $W^{1,p}_{\pi}$. Therefore, up to a subsequence, it converges weakly in $W^{1,p}_{\pi}$ to some ψ. By Remark A.1 and the compact Sobolev embedding theorem, $\psi_n \to \psi$ in L^p_{π} strong (eventually up to another subsequence). In particular, $||\psi||_{0,p,\Omega_c} = 1$. By a similar argument, as $q < p^{\star\star}$, $\mathrm{tr}\psi_n \to \mathrm{tr}\psi$ strongly in $L^q(\Gamma_c)$, and from $N_{p,q}(\psi_n) \to 0$, we obtain $\psi \in W^{1,p}_{\pi,0}$. Finally, always by $N_{p,q}(\psi_n) \to 0$ and $||\nabla\psi||_{0,p,\Omega_c} \leq \liminf_{n\to\infty} ||\nabla\psi_n||_{0,p,\Omega_c}$ since $\psi_n \to \psi$ weakly in $W^{1,p}_{\pi}$, $||\nabla\psi||_{0,p,\Omega_c} = 0$, and by Poincaré's inequality, $||\psi||_{0,p,\Omega_c} = 0$, which is in contradiction with $||\psi||_{0,p,\Omega_c} = 1$, hence (A.14), ending the proof. □

Remark A.2. *The application $N_{p,q}$ is also a norm on $W^{1,p}(\Omega_c)$, equivalent to the standard $W^{1,p}$ norm.*

Space for the velocity. The boundary condition $\overline{\mathbf{v}} \cdot \mathbf{n} = 0$ at $z = z_0$ and $z = L_z - z_0$ must be considered in the functional setting. We remark that if $\mathbf{w} = (w_x, w_y, w_z)$ is a vector field defined over $\mathbb{R}^2 \times [z_0, L_z - z_0]$ that satisfies $\mathbf{w} \cdot \mathbf{n}|_{z=z_0} = \mathbf{w} \cdot \mathbf{n}|_{z=L_z-z_0} = 0$, then $w_z(x, y, z_0) = w_z(x, y, L_z - z_0) = 0$. In other words, $w_z|_{\Gamma_c} = 0$. Therefore, according to this fact and in view of the standard variational formulations involved in the general Navier-Stokes equations framework, we are led to seek for the mean velocity in the space

$$W = H^1_{\pi} \times H^1_{\pi} \times H^1_{\pi,0}, \tag{A.15}$$

Note that the proof of Lemma A.1 combined with Korn's inequality (see [11, Appendix A]) shows that W equipped with the scalar product

$$(\mathbf{u}, \mathbf{w}) = \int_{\Omega_c} D\mathbf{u} : D\mathbf{w} + \int_{\Gamma_c} \mathrm{tr}\mathbf{u} \cdot \mathrm{tr}\mathbf{w}, \tag{A.16}$$

is a Hilbert space, and that the norm $\mathbf{u} \to \sqrt{(\mathbf{u}, \mathbf{u})}$ is a norm on W equivalent to the standard H^1 norm.

A.3 Weak solutions

Weak solutions are solutions of the variational problem deduced from the initial boundary value problem. They are usually deduced from à *priori estimates*, based on the Stokes formula and interpolation inequalities. Given the previous studies and the results already known, we must:

i) Study the action of general operator $\psi \to -\nabla \cdot (A\nabla\psi)$ on the $W^{1,p}_{\pi}$-spaces, for any positive definite matrix $A = A(\mathbf{x})$ of class C^1, periodic in the (x, y)-axes,

ii) Set the appropriate variational formulation for the system (2.16) and check that it falls within the framework of problems already studied before, in particular the one considered in [11, Chapter 7],

iii) Check if $W^{1,q}$ $(1 \leq q < 3/2)$ estimates "à la Boccardo-Gallouët" (see the initial paper [7]) can be deduced from the equation satisfied by k.

From now, the source term $\mathbf{f}$ in (2.16) is in the dual space W'.

A.3.1 Turbulent operator

In this section, $A = A(\mathbf{x})$ is a C^1 (x, y)-periodic matrix, positive definite uniformly in $\mathbf{x} = (x, y, z) \in \Omega_c = \mathbb{R}^2 \times [z_0, L_z - z_0]$, that is

$$\forall\, \mathbf{u} \in \mathbb{R}^3, \quad \forall\, \mathbf{x} \in \Omega_c, \quad (A(\mathbf{x})\mathbf{u}, \mathbf{u}) \geq \nu|\mathbf{u}|^2. \tag{A.17}$$

Let $\psi, \phi \in \mathcal{W}$. By the Stokes formula over Ω_c, which is a Lipchitz domain, we have

$$\int_{\Omega_c} -\nabla \cdot (A\nabla\psi)\phi = -\int_{\partial\Omega_c} \phi A\nabla\psi \cdot \mathbf{n} + \int_{\Omega_c} A\nabla\psi \cdot \nabla\phi. \tag{A.18}$$

Using the notations of figure 2, we decompose the integral on $\partial\Omega_c$ as

$$\int_{\partial\Omega_c} = \int_{\Gamma_c} + \int_{\Gamma_e} + \int_{\Gamma_s} + \int_{\Gamma_{lg}} + \int_{\Gamma_{lr}} \tag{A.19}$$

We have: $\mathbf{n}|_{\Gamma_e} = -\mathbf{n}|_{\Gamma_s}$ and $\mathbf{n}|_{\Gamma_{lg}} = -\mathbf{n}|_{\Gamma_{lr}}$. As $\phi A\nabla\psi$ is a C^1 function, periodic in the (x, y)-axes, we also have $\phi A\nabla\psi|_{\Gamma_e} = \phi A\nabla\psi|_{\Gamma_s}$ as well as $\phi A\nabla\psi|_{\Gamma_{lg}} = \phi A\nabla\psi|_{\Gamma_{lr}}$. Therefore, aside the term on Γ_c, all other terms in the boundary integral (A.19) are vanishing, hence (A.18) yields

$$(-\nabla \cdot (A\nabla\psi)\phi, \phi) = \int_{\Omega_c} -\nabla \cdot (A\nabla\psi)\phi = -\int_{\partial\Gamma_c} \phi A\nabla\psi \cdot \mathbf{n} + \int_{\Omega_c} A\nabla\psi \cdot \nabla\phi. \tag{A.20}$$

Unfortunately, the operator

$$\begin{cases} \mathcal{W} \to L^p(\Gamma_c), \\ \psi \to \mathrm{tr}(A\nabla\psi) \cdot \mathbf{n} \end{cases}$$

is not bounded, whatever the choice of $p \geq 1$. Therefore, Formula (A.20) cannot be extended for any ψ and ϕ in $W^{1,p}_{\pi}$ spaces. However, the structure of our problem suggests to introduce the following. Let $F : \mathbb{R} \to \mathbb{R}$ be a function which satisfies the growth condition

$$|F(\psi)| \leq C(1 + |\psi|^q), \tag{A.21}$$

for some q that be specified later, and let us consider

$$\mathcal{M}_F = \{\psi \in \mathcal{W};\ \mathrm{tr}(A\nabla\psi) \cdot \mathbf{n} = -F(\psi)\}.$$

Let M_F denotes the adherence of $\mathcal{M}_F$ with respect to the $W^{1,p}$ topology. For $\psi \in M_F$, $\phi \in W^{1,p'}_{\pi}$, the equality (A.20) becomes

$$(-\nabla \cdot (A\nabla\psi)\phi, \phi) = \int_{\partial\Gamma_c} \phi F(\psi) + \int_{\Omega_c} A\nabla\psi \cdot \nabla\phi. \tag{A.22}$$

We observe on one hand that as $\nabla\psi \in L^p(\Omega_c)$ and $\nabla\phi \in L^{p'}(\Omega_c)$, the volume integral in (A.22) is also well defined as soon as $A \in L^{p'}(\Omega_c)$. On a second hand, straightforward calculations based on Hölder and Sobolev inequalities, yield the following rules for the right choice of q to make the boundary integral well defined in (A.22):

$$\text{(A.23)} \qquad \begin{cases} \text{if } 1 \le p < 3/2, & q \le p^{\star\star} = \dfrac{2p}{3-p} = q_c, \\ \text{if } p = 3/2, & q < 2 = q_c, \\ \text{if } 3/2 < p < 3, & q \le \dfrac{3}{3-p} = q_c. \end{cases}$$

In the equation for $\overline{\mathbf{v}}$[8], $A = (2\nu + \nu_t(k))\mathrm{Id}$, $p = 2$ and

$$\text{(A.24)} \qquad F(\overline{\mathbf{v}}) = \alpha_v |\overline{\mathbf{v}}| \overline{\mathbf{v}}.$$

then $q = 2$ and $q_c = 3$. This case is well covered by the classification (A.23). In the k-equation[9], $A = (\mu + \mu_t(k))\mathrm{Id}$, $p = 3/2^-$,

$$\text{(A.25)} \qquad F(k) = \alpha_k k \sqrt{|k|},$$

then $q = 3/2$ and $q_c = 2$, which is also well covered by the classification (A.23).

A.3.2 Variational formulation

For the sake of simplicity, we only consider the case of bounded eddy viscosities. We define the following operators, suggested by the results of the previous section:

$$\text{(A.26)} \qquad \begin{cases} a(\mathbf{v},\mathbf{w}) = 2\nu \displaystyle\int_{\Omega_c} D\mathbf{v} : D\mathbf{w}, & a_e(k,l) = \mu \displaystyle\int_{\Omega_c} \nabla k \cdot \nabla l, \\ s(k;\mathbf{v},\mathbf{w}) = \displaystyle\int_{\Omega_c} \nu_t(k) D\mathbf{v} : D\mathbf{w}, & s_e(k;q,l) = \displaystyle\int_{\Omega_c} \mu_t(k) \nabla q \cdot \nabla l, \\ G(\mathbf{v},\mathbf{w}) = \alpha_v \displaystyle\int_{\Gamma_c} \mathbf{v}|\mathbf{v}|\mathbf{w}, & G_e(k,l) = \alpha_k \displaystyle\int_{\Gamma_c} k\sqrt{k}\, l. \end{cases}$$

As we are not working with a space of free divergence field, following [11, Chapter 6], we use the transport operator $b(\mathbf{z};\mathbf{v},\mathbf{w})$ defined by

$$\text{(A.27)} \qquad b(\mathbf{z};\mathbf{v},\mathbf{w}) = \frac{1}{2}\left(\int_{\Omega_c} (\mathbf{z}\cdot\nabla)\mathbf{v}\cdot\mathbf{w} - \int_{\Omega_c} (\mathbf{z}\cdot\nabla)\mathbf{w}\cdot\mathbf{v} \right).$$

By similar calculations as those carried out in section (A.3.1) and arguments of the proof of Lemma 6.3 in [11], we easily get:

Lemma A.2. *The form $(\mathbf{z},\mathbf{v},\mathbf{w}) \to b(\mathbf{z};\mathbf{v},\mathbf{w})$ verifies the following properties.*

i) b is trilinear and continuous on $(H^1_\pi)^3$, then on W, and in particular,

$$\text{(A.28)} \qquad \forall\, \mathbf{z},\ \mathbf{v},\ \mathbf{w} \in (H^1_\pi)^3, \quad |b(\mathbf{z};\mathbf{v},\mathbf{w})| \le C\, \|\mathbf{z}\|_{1,2,\Omega_c}\, \|\mathbf{v}\|_{1,2,\Omega_c}\, \|\mathbf{w}\|_{1,2,\Omega_c},$$

for some constants C only depending on Ω.

[8] Things are a little bit more technical with vector fields and laws such as (1.2), but the calculation and the final result are similar to the scalar case, changing ∇ by D, and thus we will not repeat it.

[9] When we write $k \in W^{1,\frac{3}{2}^-}_\pi$, we mean $k \in \bigcap_{r<3/2} W^{1,r}_\pi$. When we write $q \in W^{1,3^+}_\pi$, we mean $q \in \bigcup_{\rho>3} W^{1,\rho}_\pi$

ii) b is antisymmetric,

$$\forall\, \mathbf{z},\ \mathbf{v},\ \mathbf{w} \in (H^1_\pi)^3, \quad b(\mathbf{z};\mathbf{v},\mathbf{w}) = -b(\mathbf{z};\mathbf{w},\mathbf{v}), \tag{A.29}$$

iii) we also have

$$\forall\, \mathbf{z},\ \mathbf{w}\ \in (H^1_\pi)^3, \quad b(\mathbf{z};\mathbf{w},\mathbf{w}) = 0. \tag{A.30}$$

iv) For any $\mathbf{z} \in W$ such that $\nabla \cdot \mathbf{z} = 0$ (in L^2_π), we have

$$\forall\, \mathbf{v},\ \mathbf{w}\ \in (H^1_\pi)^3, \quad b(\mathbf{z};\mathbf{v},\mathbf{w}) = \int_{\Omega_c} (\mathbf{z}\cdot\nabla)\,\mathbf{v}\cdot\mathbf{w}, \tag{A.31}$$

as well as

$$\forall\, \mathbf{w}\ \in (H^1_\pi)^3, \quad b(\mathbf{z};\mathbf{z},\mathbf{w}) = -\int_{\Omega_c} \mathbf{z}\otimes\mathbf{z} : \nabla\mathbf{w}. \tag{A.32}$$

We also introduce the following transport operator, with similar properties in the appropriate spaces:

$$b_e(\mathbf{z};k,l) = \frac{1}{2}\left[(\mathbf{z}\cdot\nabla k, l) - (\mathbf{z}\cdot\nabla l, k)\right], \tag{A.33}$$

where $\int_{\Omega_c} \phi\psi = (\phi,\psi)$. More generally, given any Banach space E, $\psi \in E$, $\phi \in E'$, then so far no risk of confusion occurs, (ϕ,ψ) denotes the duality product between ϕ and ψ. These results yield the following variational problem corresponding to the system (2.16) (we write $\mathbf{v}$ instead of $\overline{\mathbf{v}}$ for the simplicity):

$$\text{Find } (\mathbf{v},p,k) \in W \times L^2_\pi \times H^{1,\frac{3}{2}^-}_\pi \text{ s.t. for all } (\mathbf{w},q,l) \in W \times L^2_\pi \times H^{1,3^+}_\pi,$$

$$b(\mathbf{v};\mathbf{v},\mathbf{w}) + a(\mathbf{v},\mathbf{w}) + s(k;\mathbf{v},\mathbf{w}) + G(\mathbf{v},\mathbf{w}) - (p,\nabla\cdot\mathbf{w}) = (\mathbf{f},\mathbf{w}), \tag{A.34}$$

$$(q,\nabla\cdot\mathbf{v}) = 0, \tag{A.35}$$

$$b_e(\mathbf{v};k,l) + a_e(k,l) + s_e(k;k,l) + G_e(k,l) = (\nu_t(k)|D\mathbf{v}|^2 - \ell^{-1}k\sqrt{|k|}, l). \tag{A.36}$$

Any solution to the variational problem (A.34)-(A.34)-(A.34) is a weak solution to the system (2.16). The calculation carried out before ensures that any strong solution to (2.16) is a weak solution. Conversely, it is easily checked that if $(\mathbf{v},p,k)$ is a weak solution which in addition satisfies $(\mathbf{v},p,k) \in (H^2_\pi)^3 \times H^1_\pi \times H^2_\pi$, and ν_t, μ_t are C^1 functions, then $(\mathbf{v},p,k)$ is also a strong solution to (2.16).

Theorem A.1. *The system (2.16) has a weak solution.*

The analysis carried out above shows that the weak formulation of system (2.16) is formulated as that considered in [11, Chapter 7], which was one of our goal. Therefore, the proof is similar to that of Theorem 7.1 in [11][10], once we will have checked that estimates "à *la Boccardo-Gallouët*" hold in this case, which is the aim of the next section.

Remark A.3. *When ν_t and μ_t are of order $k^{1/2}$ as it is the case in the real life, arguing by approximation like in section 7.5.3 in [11], we also get an existence result in which the equation for k is replaced by a variational inequality.*

Remark A.4. *It is easily proved by standard arguments that the TKE k is non negative.*

[10] In fact it is much more simpler in this case, since we do not have many additional terms coming from the boundary condition, in which $\mathbf{v}$ is involved. These terms are replaced by the boundary term $G_e(k,l)$, which is easily treated, just as the term $G(\mathbf{v},\mathbf{w})$ in the $\mathbf{v}$-equation.

A.4 Elliptic equation with a r.h.s in L^1

Basically, the k-equation is an elliptic equation with a r.h.s in L^1 (see for instance [6, 8] and in [22, Chapter 5]). Indeed, taking $\mathbf{w} = \mathbf{v}$ in (A.34) and using the result of Lemma A.2, in particular $b(\mathbf{v}; \mathbf{v}, \mathbf{v}) = 0$, we get

$$\int_{\Omega_c} (2\nu + \nu_t(k))|D\mathbf{v}|^2 + \alpha_v \int_{\Gamma_c} |\mathbf{v}|^3 = (\mathbf{f}, \mathbf{v}). \tag{A.37}$$

We deduce from Lemma A.1 combined with Korn's inequality the existence of a constant C such that

$$C||\mathbf{v}||_W^2 \leq 2\nu \int_{\Omega_c} |D\mathbf{v}|^2 + \alpha_v \int_{\Gamma_c} |\mathbf{v}|^3. \tag{A.38}$$

Therefore, by Young inequality, (A.37) yields

$$\frac{C}{2}||\mathbf{v}||_W^2 + \int_{\Omega_c} \nu_t(k)|D\mathbf{v}|^2 \leq \frac{1}{2C}||\mathbf{f}||_{W'}. \tag{A.39}$$

Hence $\nu_t(k)|D\mathbf{v}|^2 \in L^1(\Omega_c)$. The derivation of $W^{1,q}$ estimates for such an equation is based on taking $l = H(k)$ as test, for suitable continuous Lipchitz functions H. The term $-\ell^{-1}k\sqrt{|k|}$ has the correct sign, and is not involved in this process. Moreover, we also have $b_e(\mathbf{v}; k, H(k)) = 0$. Finally as $\mu_t \in L^\infty$, the term $-\nabla \cdot [(\mu + \mu_t(k)]\nabla k)$ behaves as $-\Delta k$, at least from this viewpoint. Therefore, we are left with the following basic elliptic problem:

$$\begin{cases} -\Delta k = g \in L^1_\pi, \\ \dfrac{\partial k}{\partial \mathbf{n}}|_{\Gamma_c} = -\alpha_k k|k|^{\frac{1}{2}}, \end{cases} \tag{A.40}$$

which has not been studied before, so far we know. We will have finished this section once we will have proved the following formal *à priori* estimate:

Lemma A.3. *for all $1 \leq q < 3/2$, there exists a constant $C_q = C_q(||g||_{1,1,\Omega_c})$ such that any solution k to (A.40) satisfies*

$$||k||_{1,q,\Omega_c} \leq C_q. \tag{A.41}$$

Proof. The proof follows a formal procedure, which is standard in this context. Given any $n \in \mathbb{N}$, let $H_n : \mathbb{R} \to \mathbb{R}$ be the odd continuous Lipchitz function defined by

$$\begin{cases} H_n(x) = 0 & \text{if } x \in [0, n], \\ H_n(x) = x - n & \text{if } x \in [n, n+1], \\ H_n(x) = 1 & \text{if } x \in [n+1, \infty[. \end{cases} \tag{A.42}$$

Taking $H_n(k)$ as test in (A.40) yields

$$\int_{\Omega_c} H_n'(k)|\nabla k|^2 + \alpha_k \int_{\Gamma_c} k|k|^{\frac{1}{2}} H_n(k) = \int_{\Omega_c} gH_n(k) \leq ||g||_{1,1,\Omega_c} \tag{A.43}$$

As H_n is odd, $k|k|^{\frac{1}{2}} H_n(k) \geq 0$. Therefore, (A.37) yields

$$\int_{n \leq |k| \leq n+1} |\nabla k|^2 \leq ||g||_{1,1,\Omega_c}. \tag{A.44}$$

From this estimate, we can use the result of Boccardo-Gallouët [7] turnkey to get the existence of $C_q = C_q(||g||_{1,1,\Omega_c})$ such that

$$||\nabla k||_{0,q,\Omega_c} \leq C_q, \tag{A.45}$$

for all $1 \leq q < 3/2$. To conclude, it is enough by Lemma A.1 to find an L^r estimate at Γ_c, for whatever $r < 2 = (3/2)^{\star\star}$. To do so, given any $\varepsilon > 0$, let S_ε be the odd function defined by

$$\begin{cases} S_\varepsilon(x) = \varepsilon^{-1} x & \text{if } x \in [0, \varepsilon], \\ S_\varepsilon(x) = 1 & \text{if } x \in [\varepsilon, \infty[, \end{cases} \tag{A.46}$$

and take $S_\varepsilon(k)$ as test in (A.40), which leads to

$$\int_{\Omega_c} S'_\varepsilon(k)|\nabla k|^2 + \alpha_k \int_{\Gamma_c} k|k|^{\frac{1}{2}} S_\varepsilon(k) = \int_{\Omega_c} g S_\varepsilon(k) \leq ||g||_{1,1,\Omega_c} \tag{A.47}$$

As S_ε is non decreasing, $S'_\varepsilon(k)|\nabla k|^2 \geq 0$. Hence (A.47) yields

$$\alpha_k \int_{\Gamma_c} k|k|^{\frac{1}{2}} S_\varepsilon(k) \leq ||g||_{1,1,\Omega_c}, \tag{A.48}$$

which gives by Fatou's Lemma, since $S_\varepsilon(k) \to \text{sign}(k)$ where $k \neq 0$ as $\varepsilon \to 0$,

$$\int_{\Gamma_c \cap \{k \neq 0\}} |k|^{\frac{3}{2}} \leq \liminf_{\varepsilon \to 0} \int_{\Gamma_c \cap \{k \neq 0\}} k|k|^{\frac{1}{2}} S_\varepsilon(k) \leq ||g||_{1,1,\Omega_c},$$

leading to

$$\int_{\Gamma_c} |k|^{\frac{3}{2}} \leq ||g||_{1,1,\Omega_c}, \tag{A.49}$$

hence a $L^{3/2}$ estimate for k at Γ_c, which concludes the proof. □

References

[1] Robert A. Adams and John J. F. Fournier. *Sobolev spaces*, volume 140 of *Pure and Applied Mathematics (Amsterdam)*. Elsevier/Academic Press, Amsterdam, second edition, 2003.

[2] Ricardo A. Baeza-Yates. Algorithms for string searching. In *AcM sIGIR Forum*, volume 23, pages 34–58. ACM, 1989.

[3] Anne-Claire Bennis, Tomas Chacón-Rebollo, Macarena Gómez-Mármol, and Roger Lewandowski. Numerical modelling of algebraic closure models of oceanic turbulent mixing layers. *M2AN Math. Model. Numer. Anal.*, 44(6):1255–1277, 2010.

[4] L. Berselli and R. Lewandowski. On the reynolds time-averaged equations and the long-time behavior of leray-hopf weak solutions, with applications to ensemble averages. *Preprint:* https://arxiv.org/abs/1801.08721, 2018.

[5] B. Blanke and P. Delecluse. Variability of the tropical atlantic ocean simulated by a general circulation model with two different mixed-layer physics. *J. Phys. Oceanogr.*, 23:1363–1388, 1993.

[6] L. Boccardo, J. I. Diaz, D. Giachetti, and F. Murat. Existence of a solution for a weaker form of a nonlinear elliptic equation. In *Recent advances in nonlinear elliptic and parabolic problems (Nancy, 1988)*, volume 208 of *Pitman Res. Notes Math. Ser.*, pages 229–246. Longman Sci. Tech., Harlow, 1989.

[7] L. Boccardo and T. Gallouët. Nonlinear elliptic and parabolic equations involving measure data. *J. Funct. Anal.*, 87(1):149–169, 1989.

[8] Lucio Boccardo and François Murat. A property of nonlinear elliptic equations when the right-hand side is a measure. *Potential Anal.*, 3(3):257–263, 1994.

[9] Haim Brezis. *Functional analysis, Sobolev spaces and partial differential equations*. Universitext. Springer, New York, 2011.

[10] Miroslav Bulíček, Roger Lewandowski, and Josef Málek. On evolutionary Navier-Stokes-Fourier type systems in three spatial dimensions. *Comment. Math. Univ. Carolin.*, 52(1):89–114, 2011.

[11] Tomas Chacòn-Rebollo and Roger Lewandowski. *Mathematical and Numerical Foundations of Turbulence Models and Applications*. Modeling and Simulation in Science, Engineering and Technology. Springer New York, 2014.

[12] E. Deleersnijder and P. J. Luyten. On the practical advantages of the quasi-equilibrium version of the mellor and yamada level 2.5 turbulence closure applied to marine modelling. *Applied Mathematical Modelling*, 18:281–287, 1994.

[13] Robert Eymard, Thierry Gallouët, and Raphaèle Herbin. Finite volume methods. In *Handbook of numerical analysis, Vol. VII*, Handb. Numer. Anal., VII, pages 713–1020. North-Holland, Amsterdam, 2000.

[14] Uriel Frisch. *Turbulence*. Cambridge University Press, Cambridge, 1995. The legacy of A. N. Kolmogorov.

[15] R.I Issa. Solution of the implicitly discretised fluid flow equations by operator-splitting. *Journal of Computational Physics*, 62(1):40 – 65, 1986.

[16] S. Laizet and E. Lamballais. High-order compact schemes for incompressible flows: A simple and efficient method with quasi-spectral accuracy. *Journal of Computational Physics*, 228(16):5989–6015, 2009.

[17] S. Laizet and N. Li. Incompact3d: A powerful tool to tackle turbulence problems with up to O(105) computational cores. *International Journal for Numerical Methods in Fluids*, 67:1735–1757, December 2011.

[18] M. Lee and R. D. Moser. Direct numerical simulation of turbulent channel flow up to $re_\tau = 5200$. *Journal of Fluid Mechanics*, 774:395415, 2015.

[19] S. Lele. Compact finite difference schemes with spectral-like resolution. *Journal of Computational Physics*, 103(1):16 – 42, 1992.

[20] R. Lewandowski. Long-time turbulence model deduced from the Navier-Stokes equations. *Chin. Ann. Math. Ser. B*, 36(5):883–894, 2015.

[21] R. Lewandowski and E. Odin. Turbulent systems for fluids analysed by fixed point theorems. *To appear in Pure and Applied Functional Analysis*, 2018.

[22] Roger Lewandowski. *Analyse mathématique et océanographie*, volume 39 of *Recherches en Mathématiques Appliquées [Research in Applied Mathematics]*. Masson, Paris, 1997.

[23] Roger Lewandowski. The mathematical analysis of the coupling of a turbulent kinetic energy equation to the Navier-Stokes equation with an eddy viscosity. *Nonlinear Anal.*, 28(2):393–417, 1997.

[24] Roger Lewandowski and Géraldine Pichot. Numerical simulation of water flow around a rigid fishing net. *Comput. Methods Appl. Mech. Engrg.*, 196(45-48):4737–4754, 2007.

[25] B. Mohammadi and O. Pironneau. *Analysis of the k-epsilon turbulence model*. RAM: Research in Applied Mathematics. Masson, Paris; John Wiley & Sons, Ltd., Chichester, 1994.

[26] A. S. Monin and A. M. Obukhov. Basic laws of turbulent mixing in the surface layer of the atmosphere. *Tr. Akad. Nauk. SSSR Geophiz. Inst.*, 24(151):163–187, 1954.

[27] R.-D. Moser, J. Kim, and N. Mansour. Direct numerical simulation of turbulent channel flow up to Re=590. *Physics of Fluids*, 11(4):943–945, 1999.

[28] S. Patankar. *Numerical Heat Transfer and Fluid Flow*. Series in computational methods in mechanics and thermal sciences. Taylor & Francis, 1980.

[29] Charles Pelletier. *Étude mathématique du problème de couplage océan-atmosphère incluent les échelles turbulentes*. PhD thesis, Communauté Université Grenoble Alpes, 2018.

[30] C. Peskin. The immersed boundary method. *Acta Numerica*, 11:479–517, 2002.

[31] S.-B. Pope. *Turbulent flows*. Cambridge University Press, Cambridge, 2000.

[32] L. Rossi. High order vortex methods with deforming elliptical gaussian blobs 1: Derivation and validation, 2001.

[33] P. Sagaut. *Large eddy simulation for incompressible flows*. Scientific Computation. Springer-Verlag, Berlin, third edition, 2006. An introduction, Translated from the 1998 French original, With forewords by Marcel Lesieur and Massimo Germano, With a foreword by Charles Meneveau.

[34] H. Schlichting and K. Gersten. *Boundary-layer theory*. Springer-Verlag, Berlin, enlarged edition, 2000. With contributions by Egon Krause and Herbert Oertel, Jr., Translated from the ninth German edition by Katherine Mayes.

[35] D.B. Spalding. A single formula for the law of the wall. *Transactions of the ASME, Series E: Journal of Applied Mechanics*, 28:339–391, 1966.

[36] Foken T. 50 years of the monin-obukhov similarity theory. *Boundary-Layer Meteorology*, 119:431–447, 2006.

[37] Jacques Teghem. *Recherche opérationnelle Tome1*. Ellipses, Paris, 2012.